NASA Contractor Report 191181

Isothermal Fatigue Mechanisms in Ti-Based Metal Matrix Composites

Bhaskar S. Majumdar and Golam M. Newaz
Battelle Memorial Institute
Columbus, Ohio

September 1993

Prepared for
Lewis Research Center
Under Contract NAS3-26494

National Aeronautics and
Space Administration

ISOTHERMAL FATIGUE MECHANISMS IN Ti-BASED METAL MATRIX COMPOSITES

Bhaskar S. Majumdar* and Golam M. Newaz
Battelle Memorial Institute
Columbus, Ohio 43201

ABSTRACT

Stress-controlled isothermal fatigue experiments were performed at room temperature (RT) and 538 C (in argon) on [0]8 SCS6/Ti 15-3 metal matrix composites (MMCs) with 15 and 41 volume percent SCS6 (SiC) fibers. The primary objectives were to evaluate the mechanical responses, and to obtain a clear understanding of the damage mechanisms leading to failure of the MMCs. The mechanical data indicated that strain ranges attained fairly constant values in the stress-controlled experiments at both RT and 538 C, and remained so for more than 85% of life. The fatigue data for MMCs with different volume fraction fibers showed that MMC life was controlled by the imposed strain range rather than the stress range. At RT, and at low and intermediate strain ranges, the dominant fatigue mechanism was matrix fatigue, and this was confirmed metallurgically from fractographic evidence as well as from observations of channel type dislocation structures in the matrix of fatigued MMC specimens. Reaction-zone cracks acted as important crack initiating sites at RT, with their role being to facilitate slip band formation and consequent matrix crack initiation through classical fatigue mechanisms. MMC life agreed with matrix life at the lower strain ranges, but was smaller than matrix life at higher strain ranges. Unlike the case of monotonic deformation, debonding damage was another major damage mechanism during fatigue at RT, and it increased for higher strain ranges. At high strain ranges at RT, fractography and metallography showed an absence of matrix cracks, but long lengths of debonds in the outer layers of the SCS6 fibers. Such debonding and consequent rubbing during fatigue is believed to have caused fiber damage and their failure at high strain ranges. Thus, whereas life was matrix dominated at low and intermediate strain ranges, it was fiber dominated at high strain ranges. At 538 C, the mean strain constantly increased (ratchetting) with the number of cycles. At high strain ranges, such ratchetting led to overload failure of the fibers, and debonding of the type at RT was very small. At intermediate strain ranges, fractography showed large areas of matrix cracks. However, in spite of this matrix dominated mechanism, the MMC life at elevated temperatures was significantly less than the matrix fatigue life at all strain ranges. The reason for this difference is still unclear, although metallographic and fractographic evidences suggest that internal crack initiation sites at Mo-ribbons and reaction-zone cracks may have played a critical role, with the former tending to dominate.

---

*Currently with Universal Energy Systems, Inc., Dayton, Ohio.

INTRODUCTION

Structural designs with metal matrix composites (MMCs) require not only knowledge of the material's mechanical response, but also understanding of the *inelastic deformation and failure mechanisms* . This is because the redistribution of stresses and strains between each constituent in the MMC can drastically alter the way damage and failure evolve in the MMC from one loading situation to another, requiring that the design methodology take into account all possible damage modes. Additionally, the knowledge of mechanisms help in the development of improved MMC architecture and processing routes.

In references [1-6], we had investigated the inelastic damage and plasticity mechanisms of a SCS6/Ti-15-3 MMC (a model Ti-based MMC) under tension and limited creep loading situations. In this work, we have extended the previous concepts to fatigue deformation. The overall objective was to evaluate the inelastic deformation response of a unidirectional MMC under isothermal fatigue conditions, and to obtain a good understanding of the progressive nature of plasticity and damage leading to failure of the composite. Experiments were performed at room temperature (RT) and 538 C on 0° SCS6/Ti 15-3 MMCs with both 15 and 41 volume percent SCS6 (SiC) fibers. Since the emphasis was to understand mechanisms, rather than to obtain a statistical data base, the approach involved fewer selective experiments but were followed by detailed microstructural examinations.

The fatigue response of composites can generally be divided into three regimes: Regimes 1,2 and 3 [7,8], as illustrated in Figure 1. Regime 1 is a high-stress low-life regime, during which failure is catastrophic, and probably arises because the stress in the fiber approaches its breaking strength. Regime 2 has similar characteristics as monolithic materials, and in a SCS6/Ti-6Al-4V MMC the fatigue life at room temperature was found to be comparable with that of the matrix material at strain ranges of 0.7% and below [9]. At elevated temperatures, however, the MMC life was shorter than the Ti-6Al-4V matrix life [9]. In the case of a 35 volume percent SCS6/Ti-15-3 MMC, tested at strain ranges of 0.5% and higher at RT, the MMC life was found to be shorter than the matrix life, and different matrix microstructures had little effect on MMC life [10]. For the SCS6/Ti-15-3 MMC at 300 C and 550 C [11,12], the MMC life also was shorter than the matrix life at all strain ranges, with MMC life being as much as one order of magnitude lower than matrix life at lower strain ranges at the higher temperature. Interface effects were suggested as possible reasons for the large differences in life, although the exact mechanisms were not specifically investigated. In reference [13], a life prediction approach, based on the 0° fiber stress-range was suggested, based on data obtained from different laminate configurations [13]. While there is

insufficient evidence to suggest that SCS6 fibers fail in fatigue, there is the possibility of a fiber damage mechanism (caused by the surrounding reaction zone and matrix), which may be strongly influenced by the fiber stress range. Another explanation is that the 0° fiber-stress approach may simply reflect the fact that MMC life is matrix strain-range controlled. In reference [14], recent results on the effects of volume fraction of fibers on the fatigue response of a SCS6/Ti 15-3 MMC were reported. Although fatigue life differences (for different fiber-content MMCs) were observed on a stress range basis, the data tended to collapse when compared on a strain range basis, with small differences between the data sets signifying possible effects of residual stresses and processing conditions. We shall provide comparisons between our results with those in [10,11,12,14]. In reference [15], the effects of cut/exposed fibers on fatigue life at 427 C were found not to be very significant when compared on a strain range basis. If anything, the fatigue life of a MMC with cut/exposed fibers was longer compared to the MMC with fibers not exposed to the outside. This behavior may appear rather surprising, given that the matrix life (strain controlled, R-strain=0) was much larger than MMC life (stress controlled, R-stress=0) at 427 C[11,12]. Referring back to Figure 1, Regime 3 represents fatigue lives greater than 10^6 cycles. Both crack initiation and propagation are believed to be difficult in this regime, but there is lack of data and understanding regarding mechanisms in this domain. We have not investigated Regime 3 in any detail, and shall only cursorily refer to it in this report.

A significant aspect that was lacking in the previous investigations was a detailed understanding of the inelastic deformation mechanisms leading to fatigue failure. For example, how do multiple cracks nucleate in Regime 2. In the case of monolithic materials, persistent slip bands precede fatigue crack nucleation. Do they also occur in MMCs? The results of our past investigation [1-6] on a 0° SCS6/Ti 15-3 MMC under tension loading are summarized in Figure 2, which shows that reaction-zone cracks play an important role in nucleating plasticity in the micro-yield regime of deformation (i.e. before bulk plasticity of the matrix). Those results would suggest that reaction-zone cracks also would play an important role in fatigue. Other important damage mechanisms are fiber-matrix debonding, matrix cracking, and fiber cracking, and their complex interaction in the transition regions between different fatigue regimes. The need to understand the damage mechanisms, their sequence, how they change with temperature, and how they influence mechanical responses, formed the rationale for the work described here. A preliminary assessment of results is provided in reference [16].

EXPERIMENTS

Material

Fatigue experiments were performed on 8-ply 0° SCS6/Ti 15-3 MMCs with 15 and 41 volume percent fibers; one specimen with 35 volume percent fibers also was tested. The MMCs were consolidated by Textron Specialty Metals using a foil-fiber-foil process, and all the panels utilized molybdenum (Mo) cross-weaves to hold the fibers in place during consolidation. MMCs with different volume fraction of fibers were used to obtain a clearer understanding of the fatigue damage and failure mechanisms. In addition, a few flat Ti 15-3 matrix alloy samples also were tested. The matrix material was obtained from a panel which was fabricated by HIP-ing 16 plies of matrix foils using the same processing conditions as the MMC specimens.

All tests were performed on the as-received material, without any further heat treatment. In this condition, the microstructure is relatively clean, which allows easier understanding of the effects of cyclic deformation on the dislocation structure in the MMC, and how fatigue cracks nucleate. Note that Ti-15-3 (Ti-15V-3Cr-3Al-3Sn alloy, all weight percent) is a metastable beta Ti-alloy with a body centered cubic (bcc) crystal structure, and in reference [1,6] we had shown that it contains a very fine omega (hexagonal close packed, hcp) phase which gives the material a planar slip character at room temperature. At temperatures above 300 C, acicular alpha-phase (hcp) particles are known [17,18] to precipitate in the microstructure with a fixed orientation relationship with the parent bcc phase [18]. Heat treatments at temperatures between 400 C and 550 C produce finer precipitates, and they increase the modulus by about 10 percent [17]. In most of the past fatigue studies on the SCS6/Ti 15-3 system, the MMCs were subjected to a 700 C/24 hour heat treatment with the aim of stabilizing the microstructure; such a heat treatment does not alter the modulus of the matrix alloy by any significant amount compared with the as-received material [17,19]. However, this type of heat treatment cannot prevent the formation of new finer alpha phases when the specimen is tested or held at intermediate temperatures; i.e., microstructural evolution is an integral part of the Ti 15-3 system at elevated temperatures. At the same time, as shown in reference [10], microstructural changes did not have a significant influence on the fatigue life of the alloy or MMC at room temperature. We would also like to note that in references [3,4,6] we had shown that the planar slip character of the matrix changed to a diffused non-planar slip character at 538 C. Such differences will have to be borne in mind when interpreting some of the elevated temperature fatigue results presented later.

Specimen Design

Dog-bone shaped tensile specimens were machined from SCS6/Ti 15-3 MMC panels using the electric discharge machining (EDM) technique. The surfaces and corners of the specimens were subsequently polished to reduce possibilities of major matrix cracks emanating from surface flaws. Two specimen designs were utilized, as illustrated in Figure 3. The old design involved a shoulder radius of 63.5 mm (2.5 in.). Although this design was found to be adequate for monotonic tension loading, it almost always led to shoulder failure during cyclic deformation.

The new specimen geometry, which was used for most of the experiments, had a 355.6 mm (14 in.) shoulder radius, and was based on the requirement that the maximum shear stress parallel to the fiber direction in the shoulder region not exceed 0.06 times the nominal tension stress. The number 0.06 was determined from the observed locations of fatigue cracks in the old design, and our previous experience [20] with notched MMCs, where shear stress parallel to fibers was found to have a dominant influence on major fatigue crack sites. In Figure 4, the location and size of matrix cracks in the MMC with the old design at room temperature are summarized. It was observed that although matrix cracks nucleated at angles (see Figure 4 for definition) less than 3 °, they did not grow; in fact, the density of cracks at angles between 0° and 3 ° were about the same as that in the gage section of the sample. These angles were interpreted in terms of the severity of intralaminar shear stress parallel to fibers.

In reference [21], the shear stresses in the shoulders were calculated for a specimen with 63.5 mm (2.5 inch) shoulder radius, and the value of the ratio of shear stress at shoulder surfaces to nominal tension stress (in the gage section) at two different angles are indicated by the vertical lines in Figure 4. Thus, as shown in the figure, if the ratio is less than 0.06, crack growth or premature failure at the shoulders may be avoided. The approach then was to obtain a design such that the maximum value of the ratio was less than 0.06. In reference [21], the shear to nominal stress ratios were calculated by the finite element method for a 0° tensile specimen with different shoulder radius , and these are illustrated by circular data points in Figure 5; it is worth noting that in the case of a circular hole the maximum value, obtained from simple formulas, is approximately 0.22, independent of hole radius. A least squares fit to the data points in Figure 5 indicate that a 317.5 mm (12.5 in.) root radius would likely be sufficient to maintain the ratio less than 0.06. However, in order to build in some conservativeness, while at the same time trying to keep the overall length of the sample low, a shoulder radius of 355.6 mm (14 in.) was finally selected. The locations of fractures for the two specimen geometries (see Figure 3) confirm the success of the design methodology. Slightly different specimen designs were used for 15 and 41 volume percent fibers,

both for conserving material, and for preventing slippage at the grips for the higher fiber-content MMC.

Experimental Conditions

Experiments were performed in *stress control* on a servohydraulic test system equipped with water-cooled friction grips. All tests were performed at an R-ratio of 0.1. Although specimens were cycled over a desired stress range, the strain range also remained nearly constant for better than 85% of life in all tests, at both RT and elevated temperatures. This allowed life data to be compared on a strain-range basis, as will be discussed later.

Fatigue tests were performed at RT and 538 C at a frequency of 1 Hz, so that average strain rates ranged between 5×10^{-3} and 10^{-2} /sec, depending upon the strain ranges used. The tests at 538 C were performed using induction heating in a stainless steel chamber which was initially evacuated to 10^{-4} torr of vacuum, then backfilled with argon to 1 psi gage pressure, to maintain air-tightness. A flow rate of 3 liters/minute was maintained for the argon, which was gettered in a Centorr argon purifier. The inert atmosphere was used to keep oxidation to a minimum, so that the fatigue data could be interpreted in terms of the MMC's inherent characteristics, rather than the environment.

Specimen strains (over a 12.5 mm gage length) were monitored at the specimen edges using an extensometer with ceramic arms, and the stress-strain data were recorded digitally at different fractions of life. The width and thickness strains also were monitored during two tests at RT, using a strain gage and extensometer, respectively. In [1-6] we had shown that such off-axis strains can provide useful information on whether damage or plasticity dominate during deformation. The same rationale was used here, since off-axis strains could be more sensitive than axial strains for assessing certain damage modes.

Mechanical tests were followed by detailed microstructural characterization, to identify damage and failure mechanisms. In some RT experiments, specimens were metallographically polished down to the first set of fibers before testing, and a replication technique was used to monitor the evolution of damage during cyclic loading. Transmission electron microscopy (TEM) was performed on selected specimens to evaluate the dislocation structure and any changes in the phase relationships. The fracture surfaces were examined optically and using scanning electron microscopy.

RESULTS

Mechanical Response

Mechanical Response at RT

Most of the fatigue results were obtained from MMCs with 15 volume and 41 volume percent fibers. We shall henceforth designate fiber volume fractions using the nomenclature MMC-15, MMC-41, and MMC-35, where the numbers indicate volume percent of fibers.

Figure 6 shows the effect of volume fraction of fibers on the monotonic stress-strain data at RT; the monotonic data for 15 and 35% material were generated in this program, and that for 41% MMC was obtained from [22]. The modulus values obtained from tensile tests were 133 GPa, 179 GPa, and 219 GPa for MMC-15, MMC-35, and MMC-41, respectively; these numbers were in reasonable accord with the rule of mixtures. The failure strains showed some variability, with average values indicating a slightly decreasing trend with increasing fiber volume fraction: being approximately 1.1%, 1.0 %, and 0.8 % for MMC-15, MMC-35, and MMC-41, respectively. Although lower initial compressive residual stress in the fibers is the most likely explanation for the trend in the failure strains, we would like to note that MMC-41 had more defects. These included broken Mo-weaves and, in a few places, the Mo-weave reacted strongly with the outer shell of the SCS6 fiber. These defects may also have contributed to the lower strain-to-failure of MMC-41, and possibly could influence fatigue life in the low-life/high-strain-range regime.

Another item in Figure 6 which has bearing on fatigue life is the start of non-linearity in the stress-strain curves, which was shown [1,2,5] to signify the onset of bulk plasticity in the matrix. The critical strains were approximately 0.61 %, 0.52 % and 0.48 % for MMC-15, MMC-35, and MMC-41, respectively. The trend in the values can be explained in terms of a higher average axial residual stress in the matrix with increasing volume fraction of fiber. Note that although the radial and tangential stresses in the matrix also change with the volume fraction of fibers and the applied load, those changes are small compared with corresponding changes in the axial stress in the matrix.

In order to better interpret the fatigue results presented later, we have provided, in Table 1, estimates of the residual stresses in the fiber and matrix for different volume fraction fibers and at RT and 538 C. These estimates were obtained using the FIDEP code [23], which is based on the elastic-plastic concentric cylinder model [24], and which provided excellent correlation with the

stress-strain curves in Figure 6; a processing temperature of 815 ° C was assumed. The constituent property data used in the calculations are provided in Table 2, which are based on data in [1-3,19,25-28].

Figures 7 illustrates changes in the different strain parameters as a function of fatigue cycles at RT for a MMC-15 specimen cycled at 615 MPa stress-range (≈ 0.45 % strain-range). We have also plotted the effective modulus values, which were obtained from the slopes of the straight lines joining the end-points of the hysteresis loops. For this particular stress range, there was very little hysteresis inside the loops; however, the loop widths increased with increasing stress ranges. Figure 7 shows that the strain range remained fairly constant through 90 % of life, and only in the last 10% of life did it start increasing. The strain-range increase was accompanied with a corresponding modulus decrease, and as will be shown later, such changes can be ascribed to multiple (but not numerous) cracks nucleating and propagating in the matrix. The minimum strain also increased (ratchetted) towards the end of life, and may have occurred because of prevention of crack closure during the unloading portion of a cycle. Thus, the observed large increase in maximum strain towards the end of life likely were caused by two factors: (i) decrease in the specimen stiffness because of matrix cracking, and (ii) increase in the minimum strain because of resistance to crack closure.

It is also significant that the maximum strain, within a few cycles of failure, was approximately 0.95 %, close to the failure strain of a MMC-15 monotonic tension specimen. In most other specimens, the maximum strain at failure ranged between 0.8 and 0.95 %, although there was no correlation between the maximum strain and specimen life. It appears that by a combination of matrix cracking and ratchetting (due to crack closure effects), the failure strain of the fibers was reached, which then resulted in specimen failure. It is also likely that final failure was governed by the attainment of a critical stress intensity factor, rather than a gross failure strain of the specimen, although the two are in some ways related. For example, a model [29] for crack growth for 0° MMC is based on the requirement that fracture occurs on attainment of a critical strain (corresponding to the failure strain of fibers) within a short distance ahead of the crack tip; thus, in the small fatigue samples, at least a few fibers must have reached their critical failure strain, and these may have influenced the measured maximum strain at specimen failure.

Figure 8 shows data for another MMC-15 specimen, where the width and thickness strains also were monitored. This specimen failed in 5295 cycles, and the stiffness losses towards the end of life were less than that for a specimen that lasted approximately 30,000 cycles, suggesting a smaller amount of matrix cracking before overload failure. The width and thickness Poisson's

ratio also showed a decrease towards the end of life, consistent with the observed modulus decrease, and the expectation that the Poisson's ratio should decrease with increased amounts of damage. However, changes in the Poisson's ratios were small.

Figure 9a shows stress-strain data for a MMC-41 specimen cycled at a stress range of 1358 MPa at room temperature. For this specimen, a stable hysteresis loop was reached within the first two cycles, and ratchetting was *not* observed, at least up to 79 percent of the life; the specimen failed at 503 cycles before the next set of data was recorded. No change in effective modulus was observed, indicating no imminent specimen failure. Figure 9b is a plot of thickness Poisson's ratio versus the number of cycles for the same specimen, and this plot shows a very significant decrease in the Poisson's ratio. Microstructural examination of the failed specimen, discussed later, did not reveal any matrix fatigue cracks, but showed a significant amount of fiber-matrix debonding and a few fiber failures away from the fracture surface. Such damage modes are not anticipated to alter the specimen compliance significantly, as was confirmed in Figure 9a. However, the large changes in Poisson's ratio were not expected, and additional experiments will have to be conducted to confirm the results. Also, they need to be complemented by elastic-plastic-damage calculations.

Figure 10 is a plot of the stress-range versus specimen life for the MMC specimens and the Ti-15-3 matrix. The plot includes data from this investigation, as well as those generated on the same system in references [10,14]; note that in those references, stress-controlled tests were performed at an R-ratio of 0 rather than 0.1, on MMC and matrix specimens that were heat treated at 700 C for 24 hours. Also, the matrix specimens had cylindrical geometry, rather than the rectangular geometry used in this investigation.

Figure 10 shows that for each volume fraction MMC, there was an approximate power-law relationship between stress range and specimen life, for lives greater than about 2000 cycles. However, there were life differences between each set of data, with MMC-41 showing a distinct advantage over MMC-15. It is this stress advantage that has guided the need to incorporate fibers into a metal matrix.

In the low life domain (<2000 cycles), life was extremely sensitive to the applied stress level, mainly because small stress changes and the possible growth of small matrix/fiber cracks could set off large-scale failure of the fibers and the specimen. An additional point to note, with reference to Figure 10, is that if experiments had been performed on only one volume fraction MMC, then stress-range may have appeared attractive as a characterizing parameter for predicting fatigue life, given the relatively narrow scatter band for a particular volume fraction MMC. On the other hand,

different life responses for different volume fraction MMCs illustrate that applied stress range is not a fundamental material parameter that controls life; hence, the usefulness of testing MMCs with different volume fraction fibers.

Figure 11 shows life data for the same specimens as in Figure 10, but on a strain-range basis. In this plot, the data for different volume fraction MMCs fall within a relatively narrow band, particularly for strain ranges below approximately 0.6%, suggesting strain-range as a fundamental parameter that controls life. Figure 11 shows that the data for the matrix material also agreed reasonably well with that for the MMCs, for strain ranges below approximately 0.5 %. From a deformation mechanism perspective, a possible implication is that fatigue life is matrix life controlled; it is well established that fatigue life of metals are strain range controlled (through inelastic plastic deformation). We shall present microstructural results later, as further evidence of the MMC life being dominated by matrix fatigue; however, matrix cracks generally initiated at reaction-zone cracks, suggesting that those regions likely experienced the largest amount of reversed plasticity.

At strain ranges between 0.5 % and 0.65%, the MMC life was shorter than the matrix life. Microstructural examinations showed that although the dominant mechanism was still matrix fatigue, both matrix crack nucleation and propagation were influenced by cracking of the fiber/matrix reaction-zone and Mo-weaves. In our earlier work [1-6] on monotonic deformation, it was shown that at strains at the knee of the stress-strain curve, there was bulk plasticity of the matrix along with greatly increased density of reaction-zone (rz) cracks. Also, fracture surfaces of tension specimens showed Mo-weaves on many of the plies, and Mo-weaves were also found cracked away from the fracture surface. The Mo-weave cracks and the greater density of reaction-zone cracks, along with their associated plasticity, may have been responsible for greatly reduced lives of MMC specimens compared with matrix material for strain ranges between 0.5 and 0.65%.

At even higher strain ranges (>0.65%), the MMC life was very low compared with the matrix. This domain comprises primarily Regime 1, and is dominated by fiber damage and failure, rather than matrix cracking. Figure 11 also shows that in this high strain-range regime, MMC-15 had a small but significant life advantage over MMC-41. One explanation for the life difference is based on the compressive residual axial fiber stress which increased with decreasing volume fraction of fibers (see Table 1) . Thus, for a given strain range or maximum strain (since the R-ratio on strain remained fairly constant in RT tests), the fibers in MMC-41 would be stressed higher than MMC-15, and likely fail earlier. For example, a 0.1% maximum-strain advantage (or 0.09% strain-range-advantage at R=0.1) at a given life, translates to a reduced maximum fiber stress of 393 MPa

(=0.001x393 GPa), which is comparable to the calculated difference in the axial residual stresses between MMC-15 and MMC-41 (see Table 1). Another explanation is that for a given applied strain, the axial matrix stress immediately surrounding a fiber is higher for MMC-41 compared with MMC-15 (see Table 1). Such a higher stress can induce greater number of reaction-zone cracks, and the debonding associated with them and consequent rubbing under fatigue would cause more widespread damage to the fibers and earlier failure. A third explanation is based on the observed incidence of greater damage of fibers at Mo-weaves in MMC-41 compared with MMC-15 in the as-received condition, and the fact that a large fraction of fiber damage at high strain ranges were found to occur at Mo-weaves. One or all the above mechanisms may have contributed to the lower life of the MMC-41 specimens at these higher strain ranges compared with MMC-15. We shall present micrographs later to show the nature of damage caused by Mo-weaves.

At the lowest strain ranges, the data for MMC-41 and the matrix appeared to match, whereas the lives of MMC-15 specimens appeared to be shorter. For example, at 0.24 % strain range, the MMC-41 material was unloaded after almost 4 million cycles and a matrix specimen was unloaded after approximately 6.3 million cycles, whereas at a strain range of 0.25%, a MMC-15 specimen failed in approximately 450,000 cycles. It is difficult to ascribe the life differences to rz cracks and interface effects, since at these levels of strains, rz cracks and localized plasticity were not observed under monotonic tension loading. It was observed that the grain sizes of the matrix material and MMC-41 were comparable, and were approximately three times smaller than that of MMC-15. Thus, the life advantage for the matrix and MMC-41 specimens at low strains could be explained simply on the basis of a grain size effect. Although additional confirmatory tests are needed, these results highlight the importance of matrix microstructure in controlling fatigue life in the low strain range regime. They suggest that for fatigue applications, significant improvements could be made by optimizing the matrix microstructure for high fatigue life and high crack growth resistance, while just satisfying the minimum strain-to-failure requirement for strength. Also, high volume fraction of fibers would be beneficial both from stress and strain range basis, in the long-life low-strain regime.

Mechanical Response at 538 C

Figure 12a illustrates the stress-strain data for a MMC-41 specimen, cycled at a stress range of 855 MPa at 538 C. This figure shows a number of features typical of all tests performed at 538 C. During the first cycle there was considerable non-recovered strain, because most of the non-linearity during initial loading was caused by plastic deformation (not damage) of the matrix [1-6]. On the second cycle, however, the stress-strain loop became essentially closed with an almost

linear elastic behavior; i.e., hysteresis was negligible. This behavior continued until failure of the specimen. At the same time, however, there was a steady increase in the minimum and maximum strains, so that although the stress-strain response inside a loop was nearly elastic, there also was an inelastic component, which was responsible for the steady increase in the mean strain (or 'ratchetting') of the MMC. As indicated in [11], it is most likely that ratchetting occurs because of time-dependent relaxation (reduction) of the tensile mean stress in the matrix; such a relaxation would necessitate that fibers take up a greater fraction of the applied load, causing them to extend and increase the mean strain.

The change in the various strain components as a function of the number of cycles, for the specimen in Figure 12a, are depicted more clearly in Figure 12b. Because of the open hysteresis loop in the first cycle (Figure 12a), the minimum and maximum strains in the first cycle were determined from only the loading portion (first half) of the first cycle; there was no ambiguity for the succeeding cycles because the loops were essentially closed. Note that because of the way the strains were obtained in the first cycle, and because the extent of inelasticity was most pronounced in the first cycle, there was always a jump in the various strain components between the first and second cycle, with the change in the minimum strain between cycle numbers 1 and 2 corresponding to the inelastic strain in the first cycle. The strains changed in a more uniform manner from the second cycle onwards.

Figure 12b shows that after a period of 5000 cycles, during which the mean strain increased almost logarithmically, the rates of increase of the strains decreased and the maximum strain reached an almost steady-state value of approximately 0.6 %. This steady state value was well below the failure strain of the MMC. Only after better than 93 % of the life did the mean strain and minimum strain show an increase, which was similar to the case of RT specimens. Based on our microstructural investigation (to be presented later), we believe that the upward trend in the minimum strain towards the very end of life was likely caused by matrix cracks, consistent with the very small dip in the specimen stiffness. These cracks were unable to close at the minimum load, thus causing a net measurable increase in the minimum strain. Also, in the case of other specimens with life in Regime 2, small strain-range increases and stiffness decreases were observed towards the very end of life, in agreement with a matrix cracking phenomenon.

Figure 12b also shows that the strain range was fairly constant at approximately 0.45% through better than 93% of specimen life, in spite of the fact that the maximum and minimum strains increased by significant amounts throughout the tests. As already indicated, this strain-range

constancy in stress-range controlled experiments allowed easier interpretation of fatigue life data in terms of strain ranges.

Figures 13a and 13b illustrate the ratchetting responses for the MMC-41 material tested at stress ranges of 1030 MPa and 424 MPa, respectively. At 1030 MPa, the mean strain very quickly settled down to a steady state value, although the maximum strain for this specimen was quite close to the monotonic failure strain of the MMC. We will show later that failure of this specimen involved a small amount of matrix cracking followed by overload fracture. For the specimen cycled at 424 MPa, the period of ratchetting was extremely long, and the maximum strain reached a value of approximately 0.4%. This specimen was unloaded after 2 million cycles and there was no evidence of matrix cracks.

Figures 14a and 14b illustrate the stress-strain data for a MMC-15 specimen cycled at a stress-range of 459 MPa. The responses were similar to those in Figure 12, consisting of a large non-recovered strain component in the first cycle, followed by a nearly linear elastic stress-strain response in subsequent cycles, and a continuous ratchetting to failure. A primary difference was that although both specimens started out at identical values of maximum strain and strain range in the first cycle, in the case of specimen MMC-15 (No.FT-2) the inelastic strain was significantly larger in the first cycle compared with MMC-41, so that by the second cycle the strain range for MMC-15 had dropped from 0.45% to 0.38%. However, the strain-range remained relatively constant from the second cycle onwards for better than 90% of life, after which there was a small increase likely caused by matrix cracking (observed microscopically). In Figure 14b, the mean strain did not level off as in the case of Figure 12b, likely because sufficient cycles had not accumulated to relax all the matrix stresses. Also, similar to the case of the MMC-41 specimen, the maximum strain at 90% of the life (24,409 cycles) and an extrapolation of the data to 29,097 cycles (failure) showed that they were well below the failure strain of the MMC, negating a failure mode based only on overload fracture. Rather, all the mechanical data and microstructural observations pointed to a matrix crack dominated damage mechanism for that specimen.

Figures 15a and 15b show the mechanical responses for a MMC-15 specimen tested at a larger stress range of 614 MPa (nominal strain range approx.0.52%). In this case, the strain-range drop after the first cycle was more significant, although once again the strain-range remained constant from the second cycle onwards, and did not show an increasing trend towards the end of life. The hysteresis loops were much wider for this specimen, implying a significant inelastic deformation in each cycle. Another notable feature of Figure 15b was that by cycle 600, the maximum strain had reached approximately 1 %, which was very close to the tensile failure strain of the MMC. Thus,

failure at 760 cycles was not surprising, and we shall provide evidence later that the fracture was caused simply by an overloading process, rather than by a combination of matrix fatigue cracking followed by overload fracture.

The stress-controlled fatigue life of MMC specimens at 538 C (R-stress=0.1) and 550 C (R-stress=0) are plotted on a strain-range basis in Figure 16, along with strain-controlled (R-strain=0) fatigue data of the matrix material at RT, 300 C, and 550 C; R-stress and R-strain correspond to R-ratios (ratio of minimum to maximum) on stress and strain, respectively. Note that the matrix data were obtained from polished cylindrical specimens, and the R-stress value was approximately 0 at RT and approximately -1 at 300 C and 500 C. MMC data for 15, 35 and 41 volume percent MMC are included in Figure 16. The results from the current investigation indicate an advantage of MMC-41 over MMC-15, in contrast to the case in reference [14], where the effects of volume fraction was negligible at 550 C. If the data only at 538 C and 550 C are considered, then they fall within a reasonably small band, suggesting once again a strain-controlled mechanism. Note also that whereas the current tests were performed in argon, the tests in reference[11,14,15] were performed in air. The life data from the current investigation and the earlier ones are not very different, and suggest that either the effect of environment was small, or that crack initiation was internal and therefore was not significantly influenced by the environment. Micrographs presented later point to the internal crack initiation mechanisms, with rz cracks and Mo-ribbon cracks acting as sites for internal crack initiation.

Another important feature of Figure 16 is that at 538 C, the fatigue life of the MMC was significantly below (by as much as two orders of magnitude) that of the matrix material. This was in contrast to the case of RT deformation, where the matrix and MMC life were similar at strain ranges below 0.5%. In fact, whereas the matrix life at 550 C was greater than the matrix life at RT, the MMC life at 550 C remained approximately the same as the MMC life at RT. As a result, the difference between MMC life and matrix life increased with temperature.

Figure 17 provides a comparison of all the data at RT, 538 C, and 550 C. For strain ranges above 0.55%, the life of MMC-15 at high temperatures was certainly degraded compared with the life at RT. The rapid ratchetting that was observed at 538 C likely was responsible for transferring stress to the fibers, and the situation was further aggravated by the lower compressive stress in the fibers at that temperature; this behavior may have caused the fibers to break earlier than at RT. There also were differences in the damage modes, as will discussed in the next section. For the 41 volume percent MMC, on the other hand, temperature appeared to have negligible effects on life

for all strain ranges. The reason for the contrasting behavior for MMC-15 and MMC-41 are not clear at present.

Before ending this section, a final point that needs to be made is whether proper comparisons, on a strain-range basis, are being made between stress-controlled MMC fatigue and strain-controlled matrix fatigue experiments. At RT, where softening/hardening and ratchetting were absent in the MMC experiments, the comparison is valid, so long as the R-strain in the matrix experiments are identical to the R-strain in the MMC experiments (where R-strain was almost equal to R-stress). In fact, at RT, the comparison would be inappropriate if R-strain=-1 was chosen for the matrix specimens. At 538 C, R-strain continually increased for the MMC specimens, so that although the matrix in the MMC was likely undergoing fully reversed stresses (similar to strain-controlled R-strain=0 matrix tests), the matrix tests did not simulate the exact behavior inside the MMC. An appropriate control experiment would be to subject a matrix specimen to a constant strain range, but to continually increase the R-strain, using R-strain data obtained from a corresponding MMC test. Although this may slightly reduce the difference in lives between matrix and MMC specimens, it is anticipated that the effect may not be large for a ductile matrix such as Ti-15-3 which deforms by diffused slip at 538 C.

Microstructure

Room Temperature

The dislocation structure of the fatigued MMC specimens (both MMC-15 and MMC-41) were inhomogeneous. In many areas, long arrays of dislocations were observed, as shown in Figure 18 for a specimen cycled to failure at a strain range of 0.45%. This type of planar slip character was similar to the case of tension loading [1,2], and in [1,6] we had explained the planarity of slip in terms of the presence of a fine, shearable omega phase (hcp) in the beta (bcc) matrix. The intense planarity of slip also led to fatigue cracks along slip bands, as we will show later in Figure 20b.

In other areas of the same sample, a channel type dislocation structure was observed, as illustrated in Figure 19. Such dislocation structures (with extremely high dislocation density in the walls) are characteristic of persistent slip bands (PSBs) in bcc metals [30], and confirm conclusively that classical fatigue mechanisms operate in the matrix of the fatigued MMC. This is an important and new finding. The PSB-type dislocation structure, together with similar lives of the matrix and MMC material at strain ranges below 0.5%, provide strong evidence that in Regime II, MMC life

is matrix fatigue controlled. As we will show later, the matrix fatigue life in the MMC was also influenced by the cracking of reaction zones and Mo-ribbons. The effects of these additional factors on MMC life depended on the imposed strain range, with the density and size of those cracks, and the likely detrimental effects of those cracks on fatigue life increasing with increasing strain ranges. In addition to the channel type dislocation structures, highly tangled dislocation arrangements also were observed, and they appeared to be precursors to a PSB structure.

Figure 20a shows multiple fatigue cracks in a MMC-15 specimen cycled at a strain range of 0.45%. Most often the matrix cracks had their origin in reaction-zone cracks and Mo-ribbon cracks, well embedded in the MMC. We confirmed these embedded crack initiation sites by polishing the faces and edges to different depths, as well as from the fracture surface. Matrix cracks also had their origin in fiber cracks at specimen corners and edges. However, even here, the matrix cracks started from reaction-zone cracks immediately adjacent to surface-cracked fibers (damaged by machining).

Figure 20b shows the matrix crack path, observed at the surface (face) of a MMC-15 specimen which was polished and etched prior to testing. The figure shows that the matrix crack tended to follow a crystallographic path, along slip bands in this planar slip material. We are not certain whether this particular matrix crack initiated from the specimen surface (face) or had initiated internally. However, as mentioned earlier, fractography and repeated polishing indicated that the primary matrix crack initiation sites were at reaction zone cracks, either internal or at machining damage related surfaces (corners and edges), rather than at the smooth specimen faces.

Figure 21 is a micrograph of the fracture surface of a specimen cycled at a strain range of 0.45%. The arrows (I) point to a number of radial fatigue cracks emanating from the reaction zone of the fiber. These cracks were transgranular with a fine faceted crystallographic appearance (see Figure 22), and only in a few areas could classical fatigue striations be observed; in some areas (particularly at Mo-ribbons) there were river markings suggesting even a quasi-brittle type of fracture. As shown in Figure 20b, the surface of the specimen showed that cracks tended to follow the slip traces, likely because of the strong planar character of slip, and the fine faceted appearance resulted as the crack wove in and out of the different parallel slip bands. A similar crack morphology was observed for the matrix specimens, although here there was a greater incidence of striations and relatively less incidence of a flat and quasi-brittle type of appearance as was observed in the MMC specimens. It is not clear whether the matrix constraint of the fibers and carbon diffusion from the fibers into the matrix (during processing) play any role in producing the

changes in the failure morphology between the MMC and matrix specimens; more investigation may be warranted here.

When observed optically, the fatigue cracks had a shiny appearance, and a fracture surface typically showed one or more major fatigue cracks which did not necessarily lie on the same plane. Also, separate crack initiation sites (from around fibers) were observed inside each of those major fatigue cracks (see places such as I in Figure 21) suggesting a crack interaction phenomenon. Throughout the fatigue crack growth region on the fracture surface, the extent of fiber pullout was extremely small compared with the case of monotonic tension failure. This small pullout occurred in spite of the fact that polishing of specimen faces to the fiber level showed extended lengths of debonds (3 to 5 fiber diameters long) on either side of the fatigue-crack plane. The small pullouts in the fatigue crack growth region is indicative of the fact that the combination of fiber stress and fiber damage (by rubbing) was most severe at the matrix crack surface regions.

In the fast fracture region, there was extensive fiber pullout. The transition between the fatigue and fast fracture regions was quite abrupt. This is illustrated in Figure 23, which shows a ductile dimple type of failure morphology in the fast fracture region (top half of micrograph) compared with a crystallographic type of fracture in the fatigue crack growth region; note also the flat and featureless (almost quasi-brittle) regions in some areas of fatigue fracture.

For specimens fatigued at 0.3 percent strain range and higher, Mo-weave cracks were observed on the fracture surface (see the wavy regions indicated by the arrow marked Mo in Figure 21). The presence of Mo-weaves on the fracture surface suggest that they likely had a detrimental influence on both crack initiation and propagation, although it is difficult to quantify the effects without testing specimens that do not have Mo cross weaves. The amount of Mo-weaves on the fracture surface generally increased with strain range, and may be indicative that the weaves played a more dominant role at higher strains. This could explain why MMC life was significantly shorter than matrix life at the higher strain ranges in Regime 2, where matrix fatigue crack was still the dominant damage mechanism; however, confirmatory experiments are necessary. It may be worth pointing out that monotonic tension tests had revealed [1,6] a detrimental influence of Mo-weave on MMC fracture. Also, fatigue experiments performed at 650 C on SCS6/Ti-15-3 MMCs, with Ti-Nb and Mo-weaves (the two weaves were present in the same panel), showed [31] that specimens with the Mo-weave had almost a 200 % reduced life compared with specimens containing the Ti-Nb weave. Thus, there is sufficient evidence to suggest that Mo-weaves are areas of weakness, both in monotonic tension and in fatigue. At strain ranges below 0.3%,

however, the fatigue fracture surfaces did not show evidence of Mo-weaves, suggesting that the stress and strain ranges were too low too cause any significant damage of the Mo-weave.

A major damage mechanism observed in the fatigued specimens was the evidence of fiber-matrix debonding. Figure 24 shows a matrix crack propagating from the left to right in the MMC specimen. There are two important points we would like to make here. One is that there was significant debonding on either side of the crack plane, extending over three to five fiber diameter lengths. Such interfacial debonds prevent fiber failures ahead of an advancing matrix crack; i.e., the debonds allow for a bridged crack. At the same time, however, extended debonds cause greater slippage, and can damage and fracture the fibers by fiber-matrix rubbing under fatigue loading; i.e., although some degree of debonding is desirable for crack bridging, there is probably an optimum length beyond which additional debond lengths may be undesirable. The determination of optimum lengths was beyond the scope of this study. In other regions, debonds were also observed around isolated fibers, where matrix cracks were not present. The number of such debonds around isolated fibers increased with increasing stress ranges. We shall present micrographs later illustrating such isolated debonds.

The second point to note with respect to Figure 24 is the debond that had occurred on the left side of the right-most fiber. This latter debond likely occurred because of the tensile field caused by the matrix crack to its left, and shear (parallel to the fibers) caused by plasticity of the matrix ahead of the main crack. The extent of this type of debonding was not always as extensive, although in most cases reaction-zone cracks were observed around the fiber immediately ahead of the main crack. In many instances, those reaction-zone cracks gave rise to individual matrix cracks, which then linked backwards with the main crack.

Figures 25a, 25b, and 25c are optical micrographs of replicas taken at the maximum load for a MMC-15 specimen cycled at a strain range of 0.3%. The face of the specimen was polished down to the first level of fibers before testing, which did damage the fibers and caused some of the fibers to fail prematurely (within 1000 cycles). The specimen life was 194,215 cycles which, surprisingly, was in agreement with data from other specimens, where the face had not been polished down to the fiber level.

The micrographs in Figure 25 illustrate the progression of damage, with the terms sb, cr, and db implying slip bands, crack, and debond, respectively. At 5000 cycles, a prematurely cracked fiber had given rise to a reaction-zone crack, which then initiated a slip band in the matrix, in a manner similar to that observed under monotonic deformation [1,2]. A debond between the two outer

layers of the SCS6 fibers may also be observed in Figure 25a, consistent with an anticipated debonding phenomenon. With continued cycling, more slip bands accumulated, and at 20,000 cycles (Figure 25b), a Mode I crack had initiated in the matrix inside those slip bands. This type of cyclic plasticity induced matrix crack initiation was the dominant mechanism at both room and high temperatures, with the rz cracks playing the role of facilitating slip band formation. The crack initiation in the matrix was followed by matrix crack propagation. Figure 25c shows the situation at an intermediate point, at 52,000 cycles. Both the cracks touching the right-most fiber had initiated before the main matrix crack had progressed all the way, and only one of those new cracks then joined up with the main crack. Similar cracking behavior, in regions ahead of the main crack, were observed in many other locations. They illustrate that localized plasticity and cracking *ahead* of the main crack also may play an important role in the fatigue crack growth process, contrary to all current models which assume apriori that the crack is always proceeding from one end to the other.

When the specimen failed, the matrix crack in Figure 25 had extended over five fibers on either side of the initiation point. But it was noteworthy that no other fibers failed in the wake. The situation was, however, different at higher strain ranges, where fibers generally started cracking (in MMC-15) in the wake, within three to four fibers from the crack tip.

In Figure 26, micrographs (a) and (b) correspond to replicas, taken at 15,000 cycles and 2,000 cycles, respectively, for a MMC-15 specimen cycled at a strain range of 0.45%. Matrix cracks may be observed in Figure 26a, at locations marked 1,2, and 3. At 2000 cycles (Figure 26b), faint slip band traces (see tip of right arrow with marker sb) may be observed initiating from reaction-zone cracks (see tip region of left arrow with marker rzc). These traces initiate from rzc of *intact* fibers, unlike those in Figure 25, where the first slip band could be traced to a fiber crack. In fact, reaction-zone cracking and slip band initiation at uncracked fibers was the rule, rather than the exception. With cycling, the slip bands in Figure 26b gave rise to the cracks in Figure 26a. Figure 26c, which is a micrograph of the actual specimen (rather than a replica) shows the situation at specimen failure. The cracks 1,2 and 3 are now clearly visible, and the entire specimen became filled with slip bands. In addition, many other fibers cracked, and these we believe occurred because the fibers were damaged when the face of the specimen was polished down to the first level of fibers prior to testing. This specimen had a life of approximately 18,000 cycles.

Thus, based on the microstructural observations, the sequence of damage in Regime 2 of fatigue life may be summarized as follows: slip band nucleation from reaction-zone cracks, surface-damaged fibers, or cracked Mo-ribbons, their accumulation to form crystallographic matrix cracks,

the propagation of those cracks accompanied by fiber-matrix debonding and fiber bridging and fiber failures in their wake, the joining up of nearby matrix cracks, and finally overload failure of the MMC. The dominant failure mechanism was matrix cracking, and, until overload fracture, fiber failure was restricted to the wake of the matrix crack. The replication experiments indicated that a matrix crack could initiate within 5 percent of life. However, we believe that this low value was caused by damage of the fiber during polishing to the fiber level. Metallographic examination of other unpolished specimens, where tests were stopped at different fractions of life, indicated that matrix cracks nucleated only between 30 and 50% of the life for specimens cycled at a strain range of 0.45%.

In Regime 1 of life, the fatigue damage mechanism was different. Figure 27 shows the microstructure of a MMC-41 specimen (No. FHT-1) that failed in 503 cycles, and was then polished to the fiber level. The figure shows extensive slip bands (one is marked sb in the figure), which had their origin both at reaction-zone cracks and grain boundaries. This type of slip activity was consistent with the fact that the maximum strain was larger than 0.8%, well above the knee of the monotonic stress-strain curve [1,2]. Unlike the case of specimens fatigued in Regime 2, no matrix cracks were observed in this specimen. The entire fracture surface indicated a ductile-dimple type of failure with extensive fiber pull-out, similar to the overload regions in other fatigue specimens. It is likely that sufficient cycles had not accumulated to initiate and grow matrix cracks before the specimen failed by overloading the fibers. However, in the absence of matrix ratchetting, (which is a high temperature phenomenon) a mechanism is required to explain why there was an overload failure after hundreds of cycles.

A characteristic feature of specimens (both MMC-15 and MMC-41) fatigued in Regime I was the occurrence of extensive debonding at the fiber-matrix interface. Figure 28a shows one such debond (db) around an isolated fiber in a MMC-15 specimen; see the dark lines with end points marked by the arrows. We have confirmed repeatedly [1-6] that the debond features, such as in Figure 28a, are not polishing artifacts. The two small rz cracks around the fiber appear to be too small to explain the significant length of the debond, which requires a fiber-matrix interfacial shear stress. Figure 28b illustrates the debonding feature around a fiber in a MMC-41 specimen. In this case, note how the debond crack has switched position through a crack in the outer ply of the SCS6 fiber. This type of debonding, involving switching of the debond plane, was more frequent, although it is not clear how the debonds grew by lengths as much as four times the fiber diameter, in the absence of a matrix crack. One tentative explanation [32] is that the outer layer of the fiber may have cracked during the tension part of a cycle because the maximum strain was quite high. On unloading to the minimum stress, the cracked surfaces likely resisted complete closure

through surface asperities, but were then forced into a buckling type of instability mode by the compression stress of the fiber (existing from thermal residual stresses). This could then introduce a large interfacial shear stress and drive/initiate debonds at the interfaces. Continued cycling beyond that point could then extend the length of the debond, both through damage of the interface and redistribution of stresses between the matrix and fibers.

Irrespective of what mechanism(s) was responsible for the extended lengths of the debond, their presence point to a local slippage at the interface during cyclic deformation. This type of slippage/rubbing at the interface can certainly damage the fiber, causing it to fail at a lower stress. In fact, tension tests performed on fibers extracted from fatigue-crack regions (at RT) in SCS6/Ti-15-3 specimens have indicated [33] fiber strengths of around 2600 MPa, compared with strengths of 3600-4200 MPa that were determined for fibers extracted from the as-fabricated material.

Figure 29a illustrates a fiber crack in a MMC-41 specimen that was cycled at high strain ranges; actually there is an additional fine fiber crack at the left of the main crack, as may be observed in the micrograph. Note also the badly damaged outer layers of the fiber at the crack site, and the significant lengths of debond along the length of the fiber. However, isolated fiber cracks of the type shown in Figure 29b were few, and in other areas isolated fiber cracks were associated with a fiber defect such as a small bulge/blip. More frequently, fiber cracks were observed at cracked Mo-weaves. Figure 29b shows a fiber crack at a Mo-weave, and it is noteworthy how the Mo-ribbon has cut/reacted through the outer layer of the SCS6 fiber during fabrication of the MMC. In this particular case, the debonding was likely aided by cracking of the Mo-weave (observed also in tension tests [1-6]), and the rubbing (during fatigue) that ensued after that probably led to failure of the fiber. Figure 29c shows another region, where now the Mo-ribbon had cracked and aided the debonds at the inner fiber surface. However, the fiber did not crack, and it is also significant that here the Mo-weave had not reacted with the outer layer of the SCS6 fiber. These series of micrographs illustrate the role of the Mo-ribbon during fatigue at high strain ranges, and point out the important need to control processing conditions and the choice of cross-weaves (avoid, if possible).

In summary, the fatigue failure in Regime 1 was dominated by fiber failure. Note that at room temperature there was no ratchetting of the specimen through relaxation of the matrix stress, so that damage of the fiber had to occur without any accumulation of strain (unlike that at elevated temperatures). The micrographs presented in Figure 29 provide some idea how damage of the fibers may have occurred, so that the specimen needed more than one cycle to fail.

Elevated Temperatures

Figures 30a and 30b show different views of the fracture surface of a MMC-41 specimen (No.FHT-3) that lasted approximately 79,000 cycles at a strange range of approximately 0.45% at 538 C; the corresponding life at RT was only 30,000 cycles. There were two major fatigue cracks in this specimens, and they lay in different planes. The region outlined by 'xyz' in Figure 30a shows a semicircular fatigue crack region, and a Mo-weave can be observed on the lower right side of the micrograph.

A cursory glance at Figure 30a would suggest that the crack may have initiated from the surface, likely from a surface defect or an oxide scale, although the experiments were conducted in high purity argon. However, closer inspection of the fracture surface did not provide convincing evidence that indeed the crack initiated from the surface and grew continuously inwards. The bulk of the fatigue fracture surface had a feathery (although not crystallographic) appearance, with striations in some regions. The markings changed orientations near the fibers, and made it difficult to detect the initiation site.

In Figure 30a, we would like to draw attention to the region enclosed in the area marked 'abcd'. The cracking morphology, with the outer curvature along 'bcd', suggests that a crack had initiated at the Mo-weave around the fiber marked 'a'. This crack then grew downwards to meet the surface. A similar feature, although not associated with a Mo-weave, is also observed at the bottom of fiber 'e'. It is also notable that these possible crack initiating sites were associated with minimum fiber pullout, whereas the row closest to the surface had a longer pullout (although less than in the fast fracture regions).

Figure 30b shows the region around a Mo-weave at a higher magnification, and suggest that fatigue cracks initiated at points A and B, and started growing upwards and downwards, respectively. The matrix cracks at A and B had crystallographic features that were different from the feathery matrix crack appearance in the rest of the specimen. Those crystallographic type features may be indicative of Stage I matrix cracks initiating from points A and B, and once again point to the cracked Mo-weave as an important crack initiating site. The intergranular type failure of the Mo-weave is also noteworthy in Figure 30b.

Metallographic examinations indicated that cracks also nucleated at surface-cracked fibers at specimen edges, as well as at cracked reaction zones and Mo-ribbons at specimen corners; those surface cracks did not grow to specimen failure. Given the limited nature of testing, we are

currently unable to provide statistical data on the different types of crack initiating sites and their frequency. However, if we confine attention only to internal crack initiating sites, their number was few, well below the number of cracks observed at RT. Additionally, most of those cracks initiated at cracked Mo-weaves rather than at reaction-zone cracks, suggesting that cracked Mo-weaves were the more potent initiating sites. In fact, rz cracks were very few at 538 C, both in this study, as well as in our previous study involving monotonic tension tests. In reference [11], the primary crack initiating sites were also found to be internal. However, numerous crack sites were observed around fibers, in contrast to this study; it is not clear if the differences were due to their 700C/24hr. heat treatment, the fact that the material had Ti-6Al-4 V weave, or that the tests were performed in air.

Figure 31 shows the fracture surface of a MMC-15 specimen (No.FT-3) that lasted only 760 cycles at 538 C at a strain range of 0.52%. The fracture was completely ductile as evidenced by the dimples, and is consistent with the fact that the specimen had reached the failure strain through a ratchetting mechanism. Thus, Regime 1 is dominated by overload fracture both at RT and at high temperatures.

Figure 32 shows the fracture morphology at the edge of a MMC-41 specimen (No. FHT-5) that failed in 2,296 cycles at a strain range of 0.61%. Except for the small region enclosed by the letters 'abcd' in the figure, the rest of the fracture was of a ductile-dimple type. The fatigue crack region in Figure 32 was associated with Mo-ribbon fracture, and observations at higher magnifications indicated almost quasi-brittle fracture in small regions of the matrix adjacent to the Mo ribbon crack. Thus, for this specimen, where life was in the transition between Regime 1 and Regime 2, limited matrix cracking was followed by fast fracture in most areas of the sample.

Another feature of specimens tested at 538 C was that debonding damage (away from any matrix crack) was significantly less than at RT, suggesting that isolated fiber damage by rubbing may be less at 538 compared with RT. One possibility for the lower debonding is that the fibers had greatly reduced compressive stress at 538 C, which made a compression-compression type of debonding event highly difficult.

Figure 33 shows the dislocation structure in a MMC-41 specimen which failed in approximately 2300 cycles at 538 C at a strain range of 0.61%. The characteristic feature was the nucleation of elongated alpha particles (white particles in the micrograph) in the beta matrix. These particles likely precipitated insitu at dislocations during the fatigue process. They were surrounded by a cluster of dislocations, which are believed to be interface dislocations needed to maintain

compatibility between the particles and the base matrix. Many of the particles were sheared, which may have been caused by the to and fro motion of dislocations during fatigue. Planar dislocation arrays, characteristic of RT deformation was rare, and deformation appeared to be more uniform. Also, channel type dislocation structures were not observed. The overall conclusion from the TEM study was that the microstructure was constantly evolving at 538 C, and that slip was more homogeneous rather than planar.

DISCUSSION

The mechanical response and damage mechanisms of a 0° SCS6/Ti 15-3 MMC were studied at room and elevated temperatures. Stress-controlled experiments were performed on different volume fraction MMCs, and comparative analyses of those results helped to obtain a better understanding of the fatigue process. The results of the study are summarized in this section, together with a discussion of factors that may have governed the observed mechanical response, specimen life, and mechanisms.

The tests at RT and elevated temperatures confirm that fatigue life can be broken up into three regimes, namely Regimes 1, 2, and 3. These regimes occupy different domains of life, and are based on different damage mechanisms. The mechanisms appear to have a generic character, and the three regimes can be identified in other MMCs, as has been attempted in other systems [8]. It is difficult to specify the exact domains for the three regimes without additional experiments, and the numbers specified here can only be considered as tentative as well as specific to the SCS6/Ti 15-3 system.

Regime 1 occupies up to 2,000 cycles, and failure occurs solely by overloading of the fibers: be it through damage of the fibers, or by stress transfer to fibers through matrix stress relaxation. Regime 2 occupies life from approximately 5,000 cycles to 500,000, and in this case the dominant failure mechanism is matrix cracking; the latter includes crack initiation and growth, and the combined effects of both are reflected in the plot of strain range versus number of cycles to failure. Crack initiation in this regime occurs by the to and fro motion of dislocations, and crack initiation sites are reaction zone cracks, Mo-weaves, and fiber cracks, the latter being restricted to surface cracked fibers from machining defects. The replica experiments confirmed that matrix crack initiation occurred through cyclic plastic deformation of the matrix; the roles of rz cracks and Mo-weave cracks were primarily to make slip band nucleation easier at those sites. The growth of the matrix cracks were likely influenced by fiber-matrix debonding, observed on either side of the crack plane. Regime 3 occupies the domain upward of 1 million cycles, where cracks do not

initiate, or even if they do initiate, they quickly become arrested. The transitions between the three regimes of fatigue are complex, and in the case of the Regime 1-Regime 2 transition, a combination of matrix cracking and fiber fracture was observed.

The life of a MMC specimen is influenced by: temperature, the MMC's defect population, the residual stress in the MMC, the matrix inelastic response including the kinetics of load relaxation at elevated temperatures, the fatigue crack initiation life and crack-growth rate for the matrix, and the incidence of other processes such as fiber-matrix debonding and fiber damage and their effect on overall life. Incorporating all these variables into a life prediction methodology is clearly a difficult task, considering especially the complexity of the MMC architecture. Fortunately, as observed in this study, the mechanisms and responses follow certain trends and can be grouped based on the regime of fatigue and temperature. These characteristic mechanisms provide a basis for a systematic approach to life prediction, which is at the same time *realistic*.

Table 3 summarizes the mechanisms and mechanical responses in the three regimes of fatigue and how they change with temperature. Essentially, there is a competition between matrix crack initiation and propagation on the one hand, and ratchetting and debonding induced damage of fibers on the other hand. Which mechanism dominates is dictated by the strain range and temperature.

With regard to the mechanical response in the stress-controlled experiments, a very characteristic feature at both room and elevated temperatures for all volume fraction MMCs and for all stress ranges, was that the strain range attained a reasonably constant value within a few cycles. This constancy continued for more than 90% of the life at RT and for an even higher life fraction at 538 C, before the strain range showed any noticeable increase due to matrix crack initiation.

The attainment of a constant strain range is believed to be due to two reasons. The most likely reason, particularly for strain ranges in Regime 2, is the fatigue-induced redistribution of residual stresses, which can drive the matrix into the realm of almost elastic deformation, without any significant inelasticity. The net result of the small matrix inelasticity, together with the fiber-dominated mechanical response of the 0° MMC, would be: (i) the absence of any significant hysteresis in a fatigue cycle, and, (ii) consequently a constancy of strain range for the nearly elastic MMC response. In fact, the hysteresis loops observed at both RT and elevated temperatures did illustrate a near elastic response, with the effective MMC modulus suggesting an effective matrix modulus between 85% and 90% of the matrix modulus in a tension test. Additionally, the loop widths were less at 538 C (where inelasticity should be larger due to creep) than at RT, reflecting

the fact that the matrix modulus was less at elevated temperature, and consequently any matrix inelasticity would have an even less influence on the fiber-dominated response of the MMC at 538 C compared with RT. The other reason for the constancy of strain range could be a rather flat cyclic stress-strain curve for the matrix material, although preliminary data in reference [34] suggest some limited hardening or softening, depending on the temperature and strain rate.

The consequence of constancy of strain range in the stress-controlled experiments was that we were able to compare fatigue life on a strain-range basis rather than only on a stress-range basis. The data from tests on different volume fraction MMCs clearly showed that strain-range was the more fundamental parameter that controlled life. This is an important conclusion of this work, and the inference would have been very difficult if the strain-range had changed constantly throughout the experiments.

There are two additional remarks that we would like to make here. The first is that the data for a given volume fraction MMC indicated that the life could be correlated equally well with the stress range as with the strain range. On the other hand, tests with different volume fraction MMCs showed that all data could only be correlated with the strain-range, rather than the stress-range. Hence, the usefulness of testing different volume fraction MMCs.

The second and more important point is that there is a metallurgical basis as to why the strain-range should be the fundamental life controlling parameter, at least for Regimes 2 and 3, and probably for the transition between Regimes 1 and 2. Our damage and failure investigation showed that although the final fracture was by the overloading of fibers, and though the stress-strain behavior was dominated by the stiff elastic fibers, it was the kinetics of matrix damage that determined when the composite failed. The fatigue literature gives overwhelming evidence that the fatigue life of a metal, intermetallic, and even an ionic crystal with strong covalency, is controlled by the imposed strain range, mainly because fatigue damage occurs through inelasticity, by a combination of dislocation nucleation, motion, and arrangement. Thus, it is not surprising that for the MMC, where matrix fatigue dominated life, that the imposed strain-range on the MMC should be the controlling parameter. A further conclusive evidence of matrix dominated life was the observation of the channel-type dislocation structure at RT, which is characteristic of the fatigue of bcc metals [30]. This finding also helped to establish a strain-range dominated life on an even firmer footing.

At elevated temperatures, if one were to observe a hysteresis loop in isolation, the impression from an almost elastic response would be that inelasticity processes were absent. On the other hand, the

combination of data from different loops illustrate the strong influence of inelasticity, which must be taken into account in any realistic model.

The ratchetting behavior at elevated temperatures can partially be explained by a stress relaxation process in the matrix, as illustrated in Figure 34. In reference [11], a concentric cylinder model was successfully used to model this relaxation process. The model did represent the trend in the mean strain reasonably well, however, better agreement is desired between the predicted and measured rates of change in mean strain. One reason may be that the relaxation data was obtained from static tests, whereas in fatigue experiments the matrix undergoes cyclic deformation. In this work, we took a back-calculation approach, to determine the stress-relaxation of the matrix from the measured change in mean strain of the MMC after the first half of the first fatigue cycle. Assuming iso-strain conditions, and assuming that all the change in mean strain ($\Delta\varepsilon^{MMC}{}_{mean}$) is due to a stress drop ($\Delta\sigma_m$) in the matrix, we have:

$$\Delta\sigma_m = \Delta\varepsilon^{MMC}{}_{mean} * E_f * V_f / (1-V_f) \qquad (1)$$

where E_f and V_f are the elastic modulus of the fiber (see Table 2) and volume fraction of fibers in the MMC; the latter being 0.15 or 0.41 for MMC-15 and MMC-41, respectively.

In Figure 35, we have plotted $\Delta\sigma_m$ as a function of fatigue cycles, and also indicated the life and V_f for each data set. Although one might anticipate that all the data should fall on a single curve that is characteristic of the relaxation process for the matrix, Figure 35 shows significant variations, the most notable one being the test at a strain range of 0.61%. The first half cycle of this test showed a very large inelasticity, including an elastic modulus of only about 170 GPa (compared with 210-220 GPa for the material), and this may have skewed the relaxation results somewhat. The rest of the data in Figure 35 do suggest stress relaxation rates that fall within a rather broad band, and have approximate logarithmic relationships to the number of cycles; our calculations using the static stress relaxation data on the matrix material in reference [35] also suggest a logarithmic response to time, independent of the initial stress level.

There are some additional points to note with reference to Figure 35. We estimate the maximum matrix stress at 538 C to be of the order of the matrix flow stress, which can range between 400 and 550 MPa at 538 C [3,4,25], depending on the strain-rate. Consequently, the maximum matrix stress relaxation that could occur, assuming a zero mean stress after relaxation, would range between 200 and 275 MPa. The data for MMC-15 indicate that this indeed was the case, with failure intervening either by matrix cracking or overload of the fibers, depending on the imposed

strain range. On the other hand, the data for MMC-41 indicate that the relaxation was significantly larger, suggesting that the matrix was forced into an apparently negative mean stress. It is difficult to rationalize this behavior, and we can only offer some explanations. One is that the fibers were also failing for the tests in Regimes 2 and 3, since this mechanism would cause an increase in the MMC mean strain without a concomitant decrease in specimen stiffness or increase in the strain range. Metallography did reveal limited fiber cracks away from the fracture surface or matrix cracks for the specimen tested at a strain range of 0.45%, although the maximum strain was only 0.6%. On the other hand, a thorough investigation of the 0.21% strain-range specimen (see Figure 35) has yet to be performed to confirm any fiber failure. Matrix cracks may also account for an increase in the mean strain through crack closure problems at the minimum strain, and because matrix cracks have a negligible effect on the fiber dominated response of the MMC, particularly at high temperatures. Another explanation may lie in the effect of alpha phase precipitation on the stress-strain response, including any volumetric change of the matrix; we anticipate such effects to be small. Overall, the data do warrant accurate assessment (including theoretical and experimental investigation) of the ratchetting process.

From a life prediction viewpoint, it is desirable to correlate MMC life with the lives of the constituents. The experiments at RT showed good agreement between MMC and matrix lives for strain ranges of 0.45% and below, when compared on a strain-range basis. These results were backed up with micrographs which showed dislocation structures in the MMC that were characteristic of persistent slip bands in bcc metals. The matrix life was higher at the higher strain ranges in Regime 2, and microstructural evidences suggest that Mo-ribbons likely played an important role in both crack initiation and propagation.

In Regime 1, on the other hand, the primary damage modes were debonding and possibly the damage of the fiber by rubbing, and it is therefore not surprising that matrix life did not agree with MMC life. Note that ratchetting was negligible at RT, and the fracture surface did not show any evidence of matrix fatigue cracking. We have offered only a tentative explanation for the debonding process in the absence of major matrix cracks.

Perhaps the greatest difficulty in correlating MMC life with the lives of the constituents lies with the high temperature data. The plots that were presented earlier show that at high temperatures the strain controlled life (R-ratio=0) of the matrix could be more than 10 times larger than the MMC life, even in Regime 2. This difference occurred despite a matrix crack dominated mechanism, as evidenced by large fatigue crack areas seen on the fracture surface of the MMC specimens. It is difficult to ascribe the difference between the matrix and MMC life to an oxidation effect, since the

current experiments were performed in high purity argon, whereas previous matrix tests were performed in air [11]. Additionally, tests performed at 427 C in air with extra layers of matrix, to prevent fiber exposure to machining damage and oxidation, showed [15] that such fiber protection, if anything, marginally decreased the life rather than increase the life. However, matrix specimens were machined in the form of smooth round bars compared to flat MMC specimens, which contained rough surfaces and stress risers at specimen corners and edges. These facts may partially explain the longer life of the matrix specimens.

At high temperatures, the matrix life increased, likely because the RT characteristics, namely, the planarity of slip and the propensity to easily form crystallographic cracks along slip planes, are greatly reduced. On the other hand, the MMC life was hardly influenced by temperature. Consequently, there was greater difference between the MMC and matrix life at higher temperatures. Our limited study reveals that Mo-weave cracks and reaction-zone cracks may have played important roles at elevated temperatures. The number of internal crack sites (both rz crack and Mo-crack) were much less at 538 C compared with RT, and it appears that Mo-ribbon cracks played a more dominant role. The ribbons appeared to crack early (mostly by intergranular failure) and those defects in turn led to crack initiation in the matrix. However, more experiments are needed to confirm the role of Mo-ribbons, considering that the current life data were not greatly different from those in [11], where the 550 C tests in air were performed with material that employed a Ti-6Al-4V cross-weave. Our current assessment of the detrimental effect of Mo-weave is in agreement with a past study [31], where control fatigue experiments at 650 C on a SCS6/Ti-15-3 MMC showed that specimens with a Mo-weave had significantly shorter fatigue life than specimens with a Ti-Nb weave.

We would like to point out that the stress-controlled experiments were performed at a load R-ratio of 0.1. The strain ranges also attained a fairly constant value in the tests, and at RT the R-ratio on strain remained close to 0.1. Thus, the RT life measured in the current stress-controlled experiments should coincide with those in strain-controlled experiments, provided the same R-ratio was maintained on the strain. At 538 C, however, stress relaxation of the matrix continuously increased the R-ratio on strain throughout the test. Under these conditions, the current life data may not agree with those from strain-controlled experiments, where the R-ratio on strain and the value of mean strain are maintained constant during a test. Note that changes in the mean strain are manifested through changes in the mean stress in the elastically deforming fibers. The latter can, in turn, influence the matrix crack growth rate: the rate either increasing or decreasing with increasing mean fiber stress, depending on the fiber damage and failure mechanism in the wake of the matrix crack. Additionally, the fiber stress would likely determine when a matrix crack (in Regime 2)

would become unstable, and cause failure. Stress and strain controlled fatigue and crack growth experiments at different R-ratios, including those under fully reversed conditions, would provide valuable information on the mean stress effect, and on new mechanisms that may operate under those conditions. Pending such information, a life prediction scheme would remain incomplete.

The sketches in Figure 36 summarize our current understanding of the sequence leading to failure of the MMC in different regimes of fatigue, and at different temperatures. It may be noted that fatigue failure is a complex process, and in MMCs it is sensitively dependent on the processing and loading histories; matrix stress relaxation, defects (such as at Mo-ribbon locations, reaction zones, etc.), environment, the mean stress/strain, and time-dependent changes in phase distributions, all can significantly influence which mechanism dominates. Therefore, the sketches in Figure 36 can only be considered as tentative.

CONCLUSIONS

In this work, stress-controlled isothermal fatigue tests were performed on a 0° SCS6/Ti 15-3 MMC at room temperature and at 538 C. The following are the conclusions:

(i) The fatigue data confirm that it is convenient to divide fatigue into three regimes of life, based on different damage mechanisms. The exact mechanisms that operate in each regime can change significantly with temperature.

(ii) Although experiments were performed in stress control with a fixed R-ratio and stress range, the strain range stabilized very quickly to a fairly constant value, and remained so for better than 90% of the life at both RT and elevated temperatures. This behavior allowed data to be interpreted in terms of imposed strain ranges.

(iii) Hysteresis loops were narrow, with the widths decreasing with increasing temperature. However, whereas the mean strains remained fairly constant in tests at RT, they increased continually during tests at elevated temperatures; i.e., ratchetting was a characteristic feature of high temperature experiments.

(iv) The data from tests at different temperatures, and on MMCs with a different volume fraction of fibers, helped to establish that fatigue life of the MMC in Regime II was controlled by the imposed strain range.

(v) At RT and at strain ranges below 0.45%, there was good agreement between the MMC and matrix life. This, together with the TEM observation of persistent slip bands at RT, and fractographic observations of matrix crack growth, provided confirmatory evidence that life in that domain was dominated by fatigue damage of the matrix.

(vi) At RT and at high strain ranges, fractography revealed overload fracture, and metallography revealed fiber cracks. The major damage mode was fiber-matrix debonding, and the consequent rubbing under fatigue may have contributed to fiber failure after a certain number of cycles.

(vii) Reaction zone cracks were found to be important crack initiating sites at both RT and 538 C, in agreement with extrapolations of the monotonic stress-strain response [1-3]. Essentially, slip bands initiated more easily at reaction zone crack sites, and repeated cycling led to matrix cracks through classical metal fatigue mechanisms. The growth of fatigue cracks, in turn, are anticipated to be adversely influenced by fiber-matrix debonding, observed on either side of the crack plane.

(viii) At 538 C and intermediate strain ranges (Regime 2 of life), the MMC life was more than 10 times lower than the matrix fatigue life. On the other hand, fractography and metallography indicated major matrix cracks, suggesting a matrix fatigue dominated damage. Both internal Mo-ribbon cracks and reaction zone cracks appeared to contribute to early MMC failure.

(ix) At 538 C and high strain ranges (Regime 1), fractography revealed overload fracture, and metallography showed fiber cracks but an absence of matrix cracks. Unlike at RT, there was very little debonding damage. Life in this domain is likely dictated by ratchetting; i.e., by the stress relaxation kinetics of the matrix.

(x) A tentative understanding has been obtained for the damage sequences in different regimes of fatigue, and at room and elevated temperatures. These have been presented schematically.

(xi) The results suggest that additional experiments and analyses are needed to assess the missing links left by this investigation. These include: (a) obtaining a clearer understanding as to why the MMC life was much shorter than the matrix life at elevated temperatures in Regime 2, (b) evaluating the exact role of cross-weaves on MMC fatigue life, (c) obtaining a better definition of the three regimes of fatigue in terms of strain ranges and life, and how the mechanisms interact in the transition regimes, (d) evaluating the effects of R-ratio on life, and comparisons with strain-controlled experiments, (e) obtaining additional data on the ratchetting response of the MMC, (f)

obtaining data on the relaxation kinetics of the matrix under cyclic loading, (g) obtaining data on crack growth rates in the matrix and MMC at different R-ratios, and augmenting them with analyses, and, (h) incorporating the mechanical responses and damage mechanisms into a realistic life prediction model, and validating the model using critical experiments.

ACKNOWLEDGMENTS

This work was supported by the NASA Lewis Research Center under Contract No.NAS3-26494. The program monitor was Dr. Brad Lerch. We gratefully acknowledge the encouragement and advice provided by Dr. B. Lerch, Dr. J.R. Ellis, and Dr. S. Arnold of NASA Lewis during this program. We also thank Drs. G. Halford, T. Gabb, and J. Gayda for providing the matrix data and for useful discussions.

REFERENCES

1. B.S. Majumdar and G.M. Newaz,"Inelastic deformation of metal matrix composites: plasticity and damage mechanisms", Philosophical Magazine, Vol.66, No.2, pp.187-212, (1992)

2. B.S. Majumdar and G.M. Newaz,"Inelastic deformation of metal matrix composites: Part I-plasticity and damage mechanisms", NASA Contractor Report No. 189095, (1992)

3. B.S. Majumdar and G.M. Newaz,"Inelastic deformation of metal matrix composites: Part II-plasticity and damage at high temperature", NASA Contractor Report No. 189096, (1992)

4. B.S. Majumdar and G.M. Newaz, and F.W. Brust,*Constitutive Behavior of High Temperature Composites,* Proceedings of ASME Winter Annual Meeting at Annaheim, CA, Eds. B.S. Majumdar, G.M.Newaz and S.Mall, MD-Vol.40, pp.77-90, (1992)

5. B.S. Majumdar, G.M. Newaz, and J.R. Ellis,"Evolution of plasticity and damage in metal matrix composites", in print, Metall. Transactions (1993)

6. B.S. Majumdar and G.M. Newaz, F.W. Brust, and J.R. Ellis,"Deformation mechanisms in a Ti-Alloy/SiC Metal Matrix Composite", Proceedings of the VII th. World Conference on Titanium held in San Diego, (1992)

7. R. Talreja, Fatigue of Composite Materials, Technomic Publishing Co., Lancaster, PA, (1987)

8. P.A. Bartolotta and P.K. Brindley, High Temperature Fatigue Behavior of a SiC/Ti-24Al-11Nb Composite, NASA Tech. Memorandum No.103157, (1990)

9. S.M. El-Soudani and M.L. Gambone,"Strain-controlled fatigue testing of SCS6/Ti-6Al-4V metal matrix composite", Fundamental Relationships Between Microstructure and

Mechanical Properties of Metal Matrix Composites, P.K. Liaw and M.N. Gungor Ed., TMS, PA, pp.609-704(1990)

10. T.P. Gabb, J.Gayda, B.A. Lerch, and G.R. Halford,"The effect of matrix mechanical properties on [0]8 unidirectional SiC/Ti composite fatigue resistance", Scripta Metallurgica, Vol.25, pp.2879-2884, (1991)

11. J.Gayda, T.P. Gabb, and A.D. Freed,"The isothermal fatigue behavior of a unidirectional SiC/Ti composite and the Ti alloy matrix", *Fundamental Relationships between Microstructure and Mechanical Properties of Metal Matrix Composites*, Ed. P.K. Liaw and M.N. Gungor, The Metallurgical Society, pp.497-514 (1990); Also, NASA Technical Publication No.101984, (1989)

12. T.P. Gabb, J.Gayda, and R. Mackay,"Isothermal and non-isothermal fatigue behavior of a metal matrix composite", J. of Composite Materials, Vol.24, pp.667-686, (1990)

13. W.S. Johnson, S.J. Lubowinski, and A.L. Highsmith,"Mechanical characterization of unnotched SCS6/Ti-15-3 metal matrix composites at room temperature", Thermal and Mechanical Behavior of Metal Matrix and Ceramic Matrix Composites, ASTM STP 1080, Eds.J.M. Kennedy, H.H. Moeller, and W.S. Johnson, pp.193-218, (1990)

14. J.Gayda and T.P. Gabb,"The effect of fiber content on the fatigue life of SCS6/Ti-15-3 composite", Proceedings of NASA HITEMP Conference No. 10104, pp.51.1-51.15, (1992)

15. J. Gayda and T.P. Gabb,"The effect of cut/exposed fibers on the fatigue life of a SCS6/Ti-15-3 composite", Proceedings of the 1991 NASA HITEMP Conference No.10082, pp.37.1-37.7, (1991)

16. B.S. Majumdar and G.M. Newaz,"Inelastic deformation of metal matrix composites: compression and fatigue", Proceedings of NASA HITEMP Conference No. 10104, pp.49.1-49.17, (1992)

17. B.A. Lerch, T.P. Gabb, and R.A. Mackay, Heat Treatment Study of the SiC/Ti-15-3 Composite System, NASA Tech. Rep. No. TP-2970 (1990)

18. J.C. Williams,,"Critical Review: Kinetics and Phase Transformations", *Titanium Science and Technology*, Vol. 3, Proc. of 2nd. International Conference on Titanium, Plenum Press, Eds. R.I. Jaffee and H.M. Burte, pp.1433-1494 (1973)

19. B.A. Lerch and J. Saltsman, *Tensile Deformation Damage in SiC Reinforced Ti-15V-3Cr-3Al-3Sn*, NASA Technical Memorandum 103620, NASA Lewis Research Center (1991)

20. G.M. Newaz and B.S. Majumdar,"Crack initiation around holes in a unidirectional MMC under fatigue loading", Engg. Fracture Mechanics, Vol.42, No.4, pp.699-711 (1992)

21. P.W. Worthem, Flat tensile specimen design for advanced composites, NASA Contractor Report No. 185261 (1990)

22. B.A. Lerch, NASA LeRC, Cleveland, Ohio, Private communications (1992)

23. D. Coker,"Finite Difference Elastic-Plastic Analysis [FIDEP]", Software code based on the concentric cylinder model, Materials Directorate, WL/MLLN, Wright-Patterson AFB, Ohio(1992).

24. C.H. Hamilton, S.S. Hecker, and L.J. Ebert,"Mechanical behavior of uniaxially loaded multilayered cylindrical composites", J. Basic Engineering, Trans. ASME, pp.661-671 (1971)

25. U. Santosh and J. Ahmad,"Metal matrix composite response under biaxial loading", *Constitutive Behavior of High Temperature Composites,* Proceedings of ASME Winter Annual Meeting at Annaheim, CA, Eds. B.S. Majumdar, G.M.Newaz and S.Mall, MD-Vol.40, pp.53-66, (1992)

26. R.P. Nimmer, R.J. Bankert, E.S. Russell, G.A. Smith, and P.K. Wright, J. Composite Technology and Research, Vol.13, pp.3-13 (1991)

27. C.A. Bigelow,"The effects of uneven fiber spacing on thermal residual stresses in a unidirectional SCS-6/Ti-15-3 laminate", J. Compos. Tech. and Research, JCTRER, Vol.14, No.4, pp.211-220 (1992)

28. N.J. Himmler,"Thermal expansion of chemicallly vapor deposited SiC fibers", Symposium on High Temperature Composites, American Soc. for Composites, Technomic Publishing Co., Lancaster, PA, pp.206-213 (1989)

29. G.J. Dvorak, Y.A. Bahei-El-Din, and L.C. Bank,"Fracture of fibrous metal matrix compoisites", Engg. Fr. Mech., Vol.34, No.1, pp.87-123 (1989)

30. H. Mughrabi, K. Herz and X. Stark,"The effect of strain rate on the cyclic deformation properties of alpha-iron single crystals", Acta Metall., Vol.24, pp.659-668 (1976)

31. M. Morasic, S. Russ, and J.M. Larsen,"The effect of cross-weaves on the mechanical behavior of beta titanium composites", Presented at the AIAA Mini-Symposium, (March 14,1991); also internal report at the WPAFB, Dayton, Ohio

32. T. Nicholas and B.S. Majumdar, WPAFB, Dayton, Ohio, Private communications (1992)

33. P.Kantzos, L.Ghosn, and J.Telesman,"The effect of degradation of the interface and fiber properties on crack bridging", Proceedings of NASA HITEMP Conference No. 10104, pp.32.1-32.14, (1992); also proceedings of the MRS Spring Meeting (1992)

34. M.E. Tuttle and J. Rogacki, Thermoviscoplastic response of Ti-15-3 under various loading conditions, NASA contractor report No. 187621, (1991)

35. J.Gayda and T.P. Gabb,"Isothermal fatigue behavior of a $[90]_8$ SiC/Ti-15-3 composite at 426 C", NASA Technical Memorandum No. 103686, (1991)

TABLE 1. CALCULATED RESIDUAL STRESSES IN SCS6/Ti-15-3 MMCs FOR DIFFERENT VOLUME PERCENT FIBERS.

Temperature °C	Volume Percent Fibers	Fiber Axial Residual Stress, MPa	Matrix Axial Residual Stress at Interface, MPa (1)	Matrix Radial Residual Stress at Interface, MPa	Matrix Tangential Residual Stress at Interface, MPa	Comments
RT	15	-735	130	-173	235	No Plasticity at Zero Load
	35	-425	229	-136	287	"
	41	-349	243	-117	284	"
538	15	-288	51	-65	89	"
	41	-133	93	-44	107	"

* Calculations performed using FIDEP [23], based on the concentric cylinder model; elastic/linearly-plastic calculations. The constitutive data, used in the model, are provided in Table 2

(1) When the matrix remains elastic, the axial residual stress in the matrix is independent of radius in the concentric linder model [24].

TABLE 2. CONSTITUTIVE PROPERTIES OF SCS-6 FIBERS AND Ti-15-3 MATRIX THAT WERE USED IN CURRENT CALCULATIONS (SEE TABLE 1).

Temperature °C	E GPa	Coefficient of Thermal Expansion, x E-06/°C	Proportional Limit, MPa	Poisson's Ratio
SCS-6 (SiC) Fiber				
25	393	4.72	-	0.19 [19]
300	383	5.03	-	"
500	375	5.36	-	"
600	371	5.44	-	"
800	362	5.66	-	"
1000	355	5.75	-	"
Ti-15-3 Matrix				
25	91	8.48	710	0.32
300	80	9.30	580	"
538	75	10.00	400	"
650	67.6	10.26	323	"
700	53	10.50	-	"
815	48	10.90	-	"

Literature review indicates a wide variation in the thermal expansion coefficient of SCS-6 fibers between RT and 400° C, with values of 4.8E-06 [13], 3.5E-06 [27], and 2.2E-06 [19,28]. There is better agreement in other fiber properties between different references.
Matrix mechanical properties at RT, 538 C, and 650 C, measured in our prior investigations [1-3]. Matrix mechanical properties at 300 C obtained from [11]. The rest of matrix properties obtained from [19]. Linear work hardening rate of matrix varied between 1 and 4 GPa.

TABLE 3. SUMMARY OF MECHANISMS AND MECHANICAL RESPONSES DURING FATIGUE AT ROOM AND ELEVATED TEMPERATURES

Temperature	Regime	Mechanisms and Material Response
RT	1	The dominant damage mechanism was overload fracture of fibers. This was preceded by extensive fiber-matrix debonding, and consequent damage of fibers by rubbing at the interface during fatigue.
RT	2	The dominant damage mechanism was matrix fatigue, involving both crack initiation and propagation. Matrix crack initiation occurred through classical plasticity mechanisms, generally at reaction-zone cracks, since those regions were preferred slip band sites in the 'micro-yield' domain. At low and intermediate strain ranges MMC life was comparable to matrix life. At higher strain ranges, MMC life was shorter, and both Mo-ribbon cracks and reaction-zone cracks played important roles here. Interfacial fiber-matrix debonding was observed, primarily next to matrix cracks, but its effects on crack growth rate and fiber damage/fracture in the wake were not examined.
RT	3	Crack initiation was difficult at such small strain ranges; consequently the MMCs showed endurance behavior. Grain size of the matrix may play an important role in this regime of fatigue.
Elevated Temperatures	1	The dominant damage mechanism was overload failure of fibers caused by a ratchetting (increase in mean strain of MMC) mechanism, through matrix stress relaxation and transfer of load to fibers. Debonding of the type at RT was small.
Elevated Temperatures	2	The dominant damage mechanism was again matrix fatigue, involving both crack initiation and propagation. Ratchetting also occurred continuously, but was insufficient to cause overload failure. MMC life was significantly shorter than matrix life. Matrix crack initiation sites were mostly internal, at Mo-ribbon cracks and reaction-zone cracks; the former appeared to dominate. Interfacial fiber-matrix debonding was observed next to matrix cracks, and they likely influenced crack growth rates.
Elevated Temperatures	3	Crack initiation and propagation was difficult, judging from near absence of cracks in this regime.

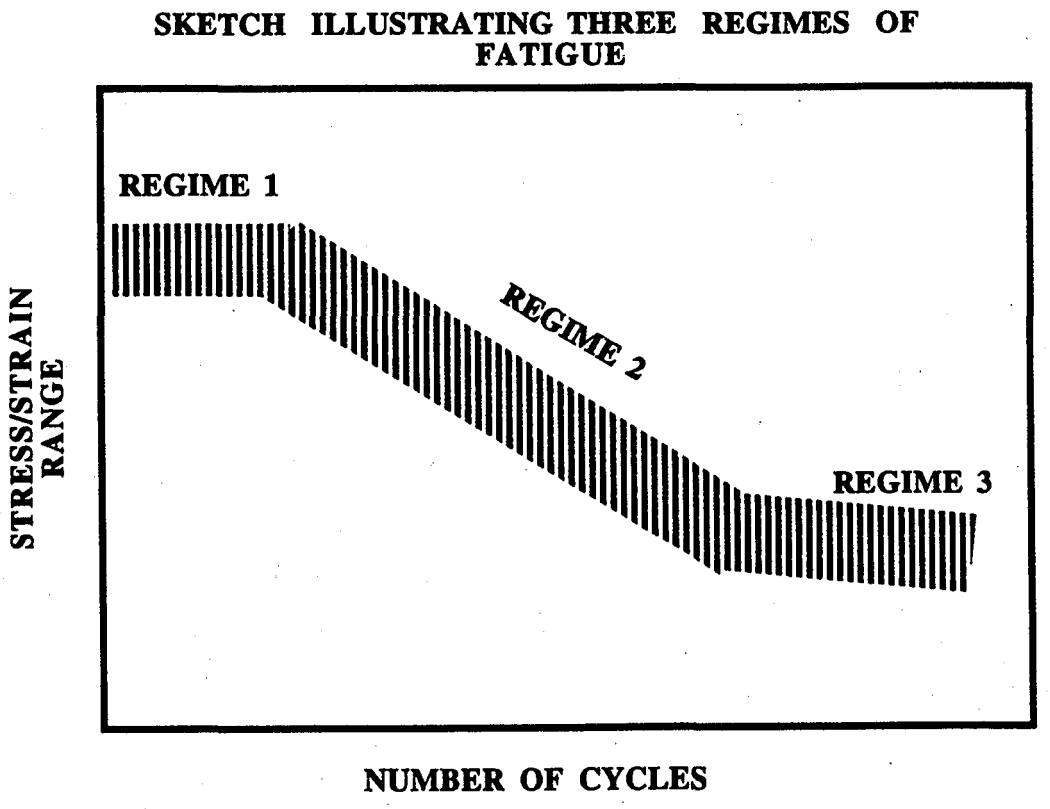

Figure 1. Sketch illustrating the three regimes of fatigue for composites.

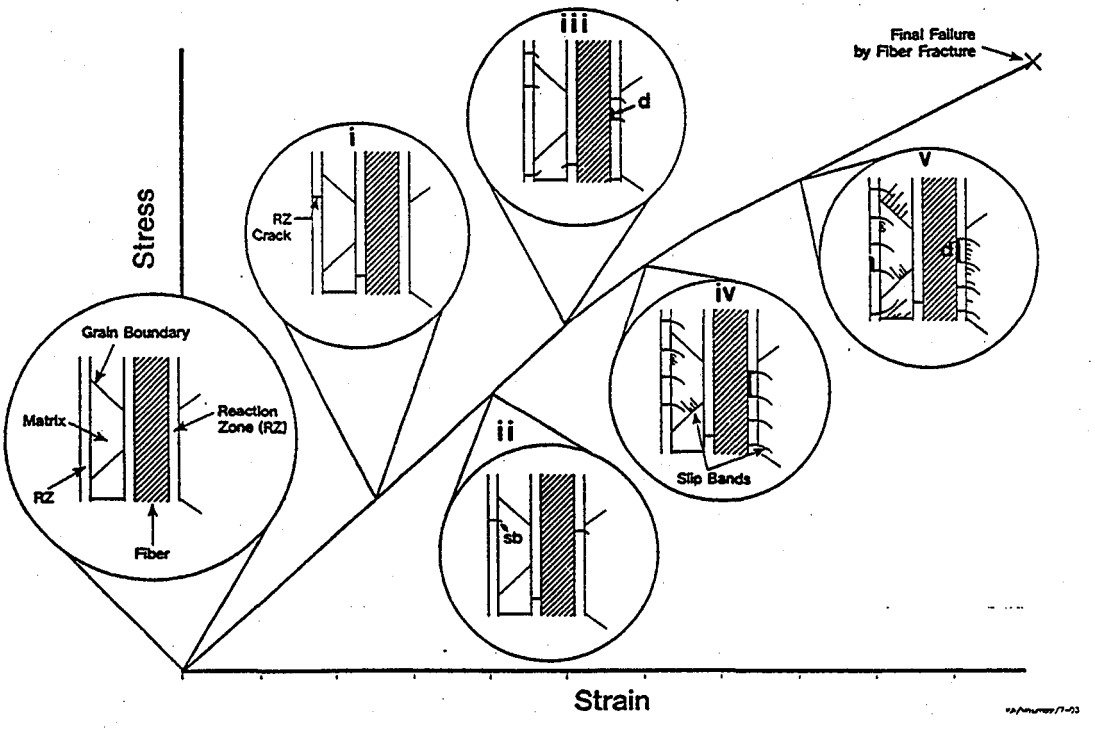

Figure 2. Sketch illustrating the progress of plasticity and damage during monotonic deformation of fiber reinforced MMCs [Majumdar & Newaz].

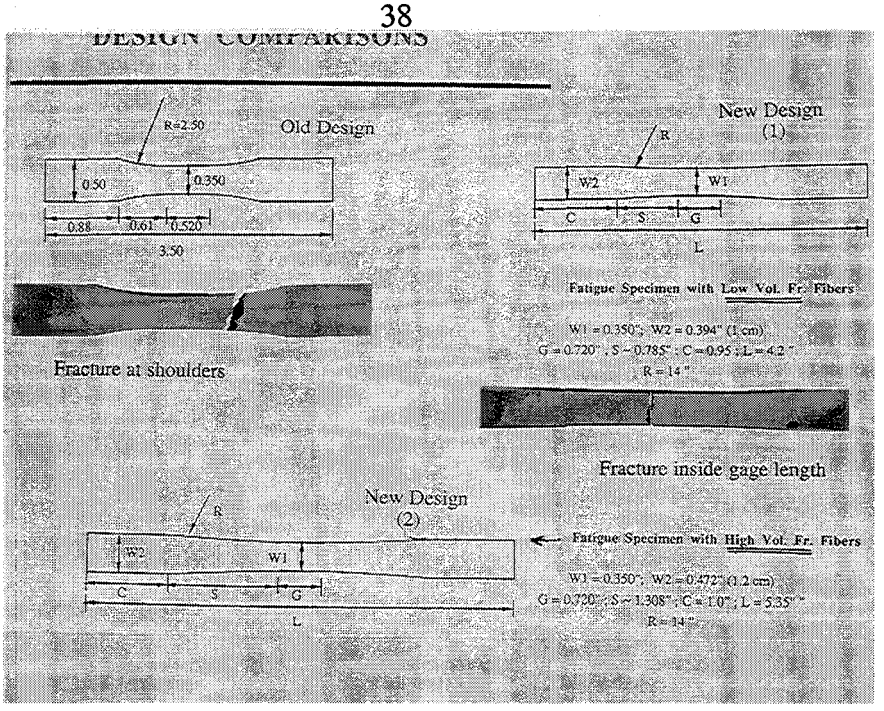

Figure 3. The figure shows different specimen designs that were used in this investigation. The one with the 2.5-inch shoulder radius corresponds to the old design, and was used only in the initial few tests.

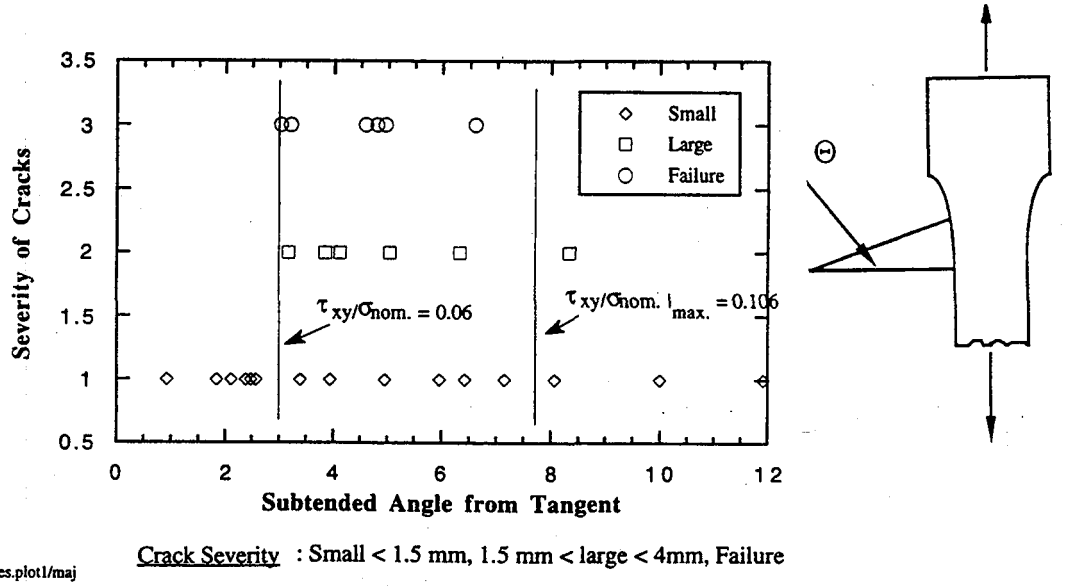

Figure 4. Sketch showing the size and locations of cracks inside the shoulders for MMC specimens (with the old design), fatigued at RT. The cracks have been classified into different size ranges, to illustrate locations where fatigue cracks propagated the most .

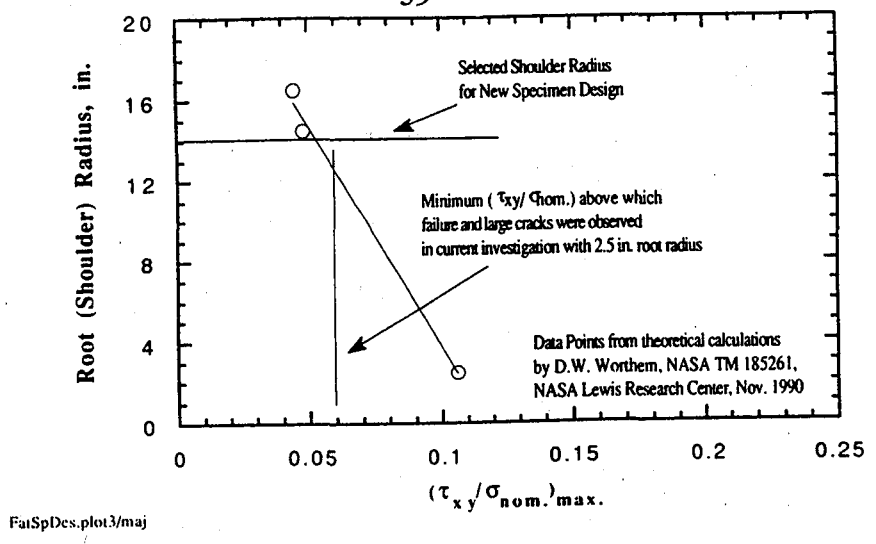

Figure 5. The design approach used to arrive at an appropriate shoulder radius, so that failure at shoulders could be avoided.

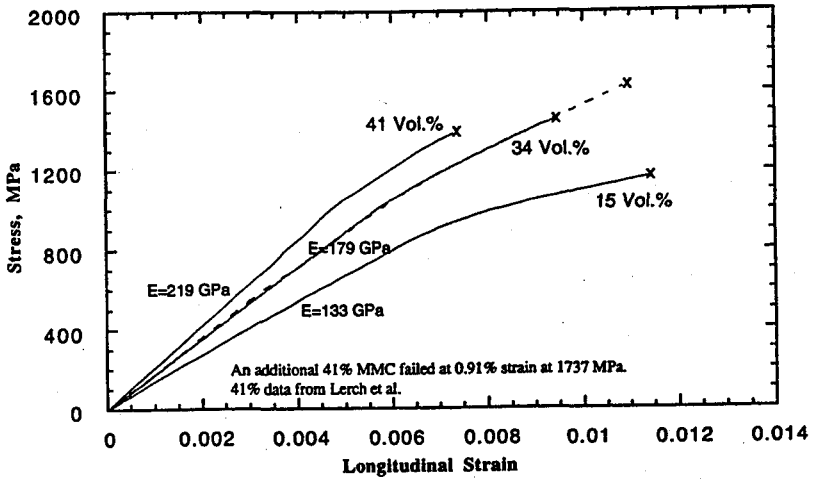

Figure 6. Stress-strain behavior at RT for 0° SCS6/Ti 15-3 MMCs with 15, 35, and 41 volume percent fibers; they are designated as MMC-15, MMC-35, and MMC-41, respectively.

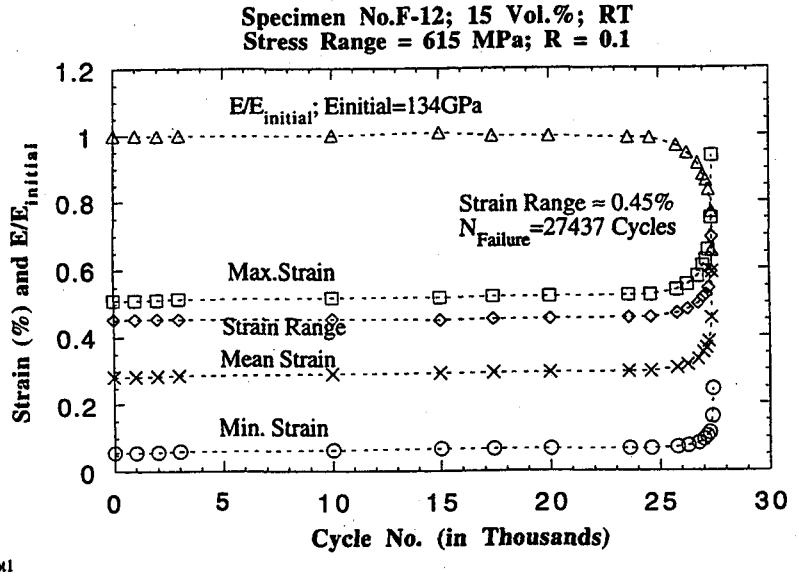

Figure 7. Evolution of the different strain parameters, and the effective elastic modulus, as a function of the number of cycles for a MMC-15 specimen, tested at RT at a stress range of 615 MPa.

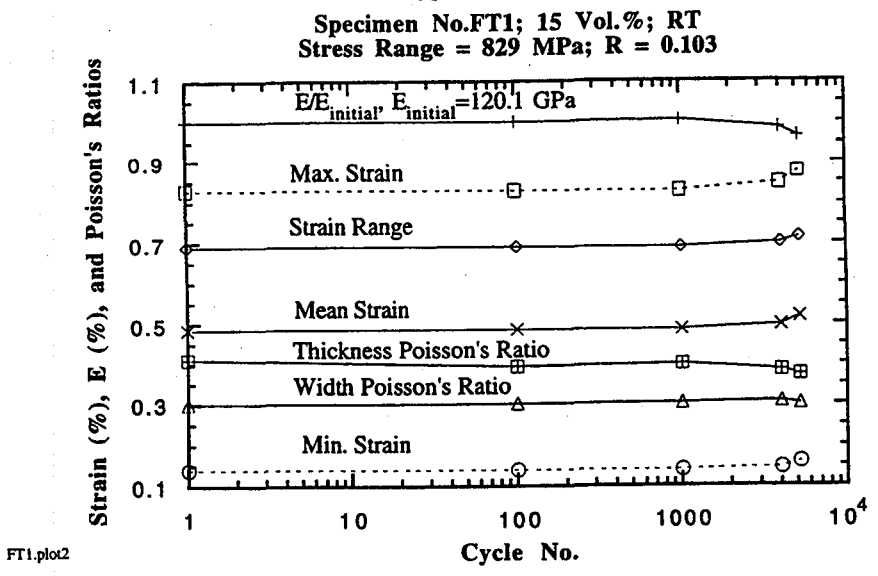

Figure 8. Evolution of the different strain parameters, and the effective elastic modulus, as a function of the number of cycles for a MMC-15 specimen, tested at RT at a stress range of 829 MPa. The changes in the width and thickness Poisson's ratios also are plotted.

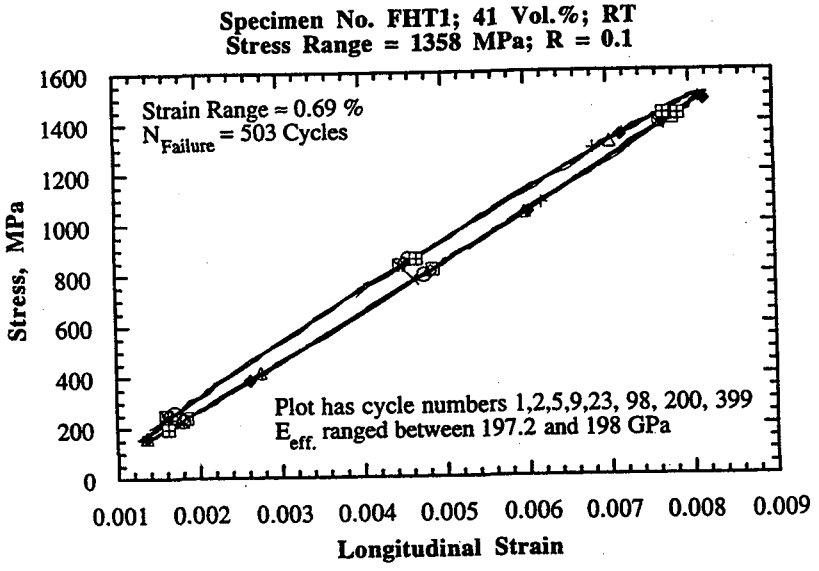

Figure 9a. Stress-strain plots for a MMC-41 specimen cycled at a stress range of 1358 MPa at RT.

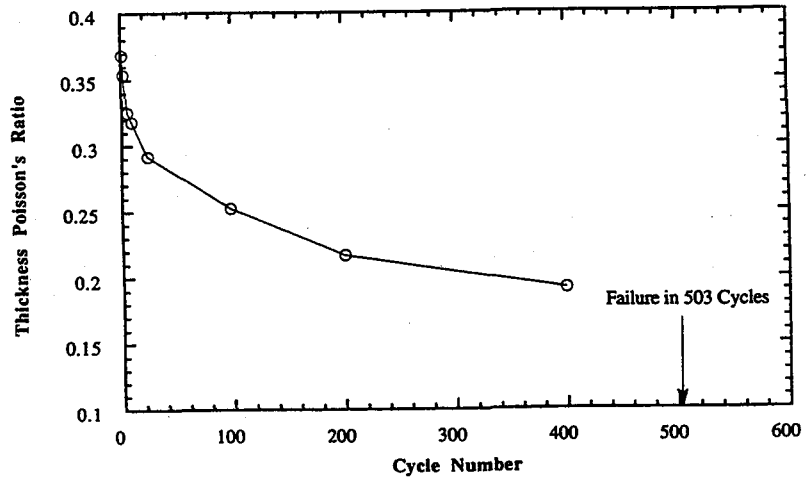

Figure 9b. Evolution of the thickness Poisson's ratio for the specimen in Figure 9a. This specimen showed significant debonding damage.

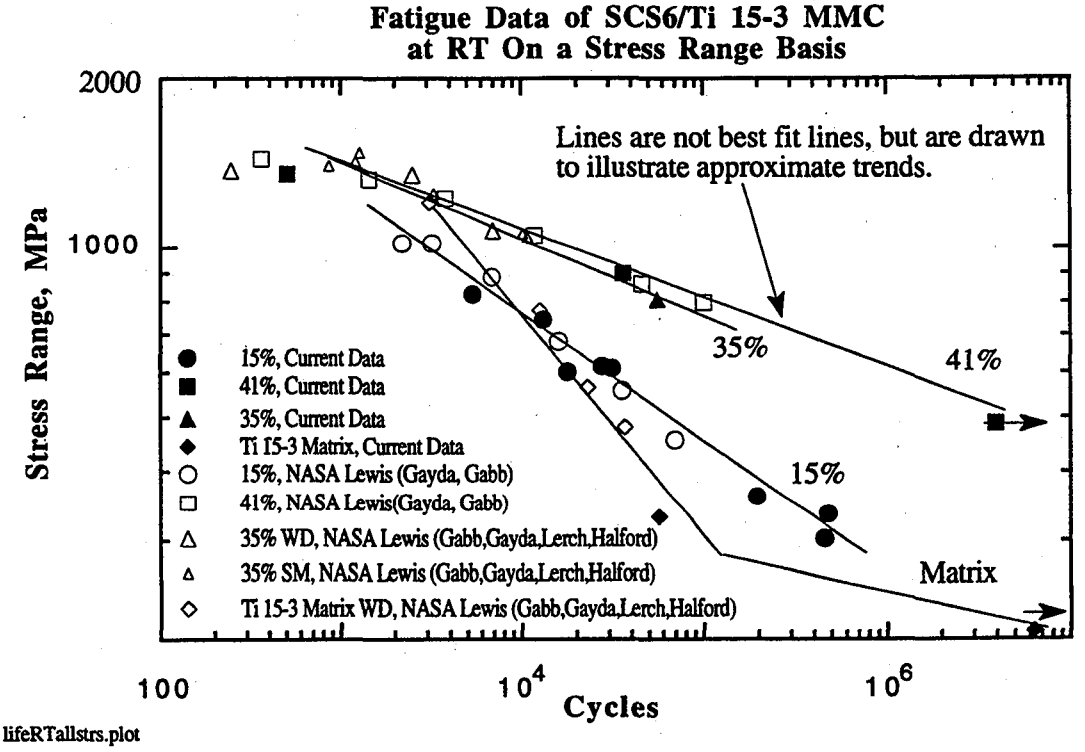

Figure 10. Fatigue life of 0° SCS6/Ti 15-3 specimen at RT, plotted on a stress range basis.

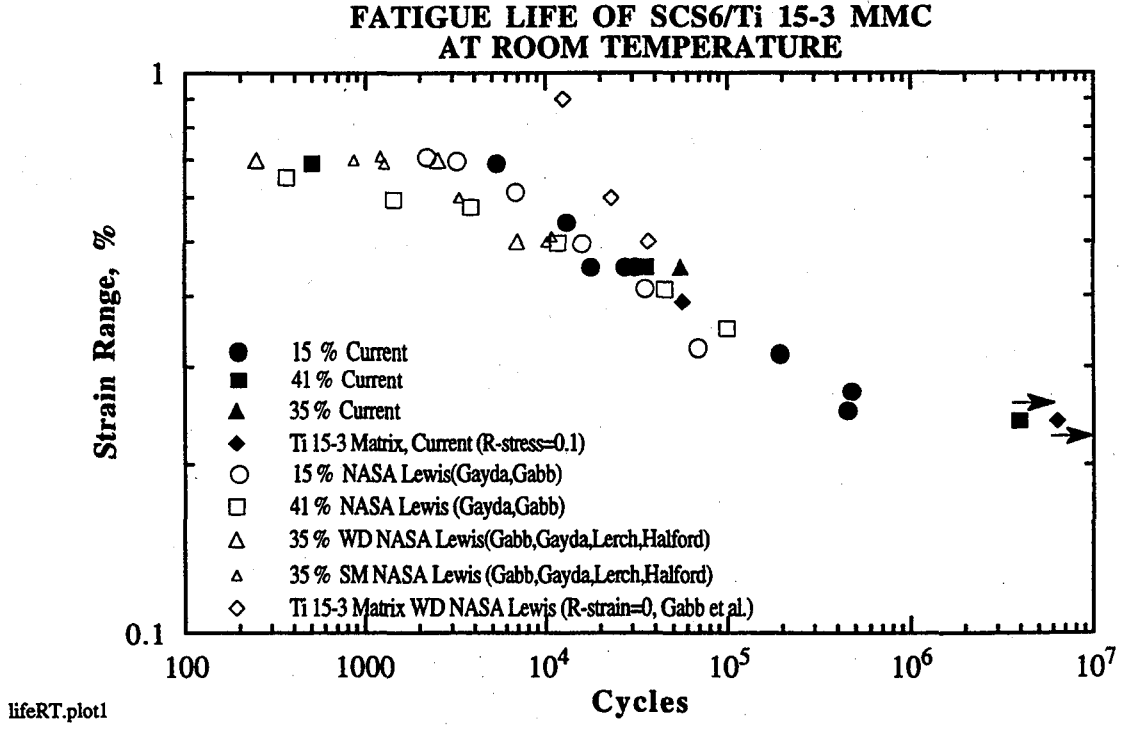

Figure 11. Fatigue life of 0° SCS6/Ti 15-3 MMC at RT, plotted on a strain range basis. Data for matrix material also are included.

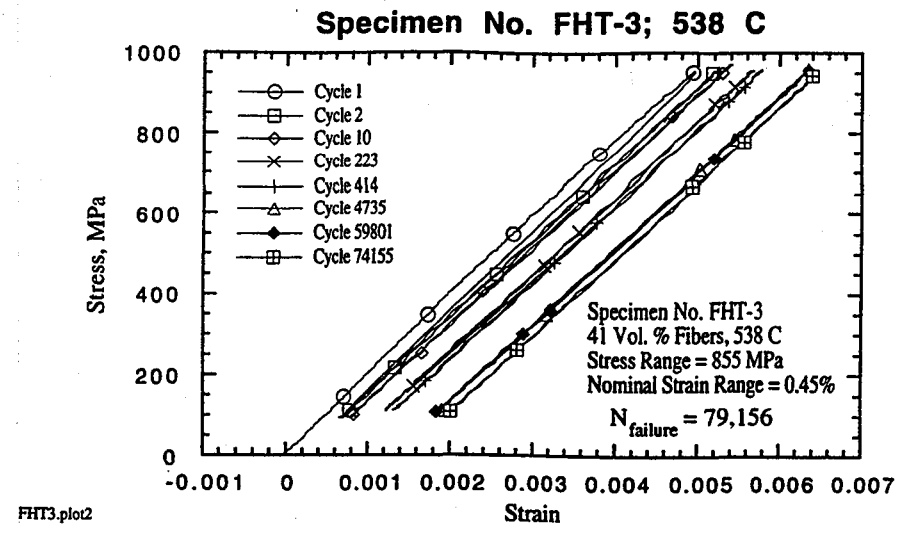

Figure 12a. Stress-strain plots for a MMC-41 specimen cycled at a stress range of 855 MPa at 538 C.

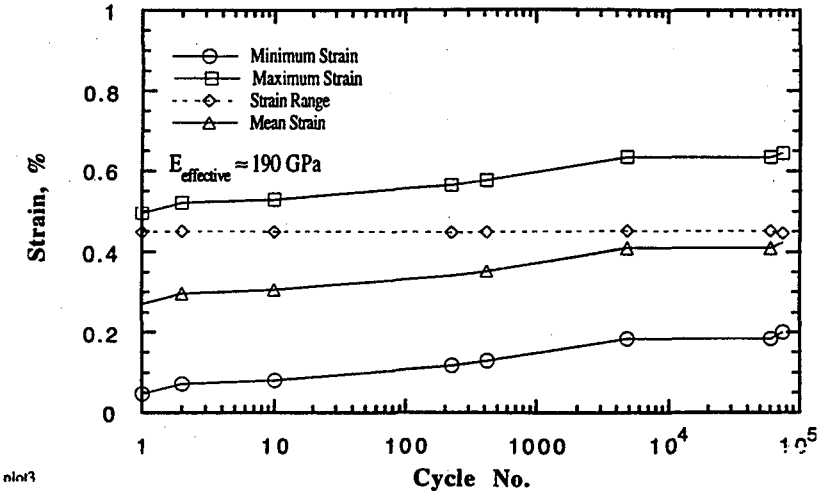

Figure 12b. Evolution of the different strain parameters as a function of the number of cycles for the specimen in Figure 12a.

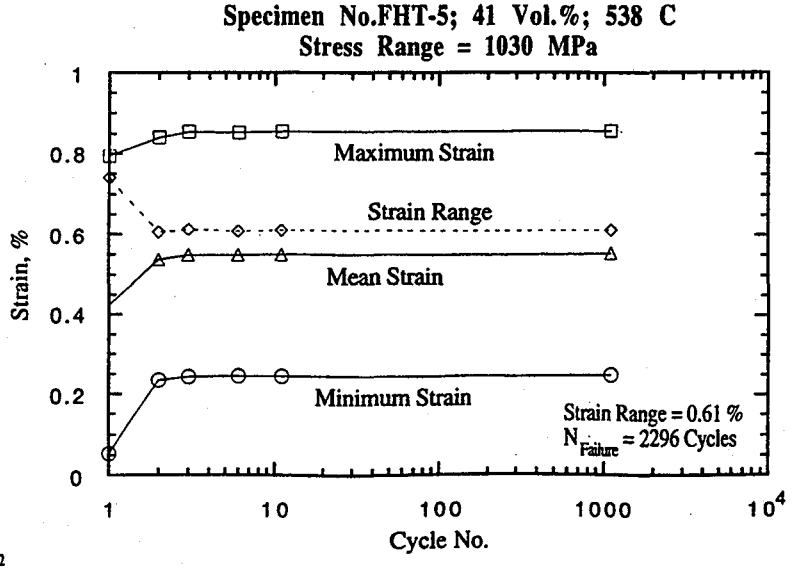

Figure 13a. Evolution of the different strain parameters as a function of the number of cycles for a MMC-41 specimen fatigued at a stress range of 1030 MPa at 538 C.

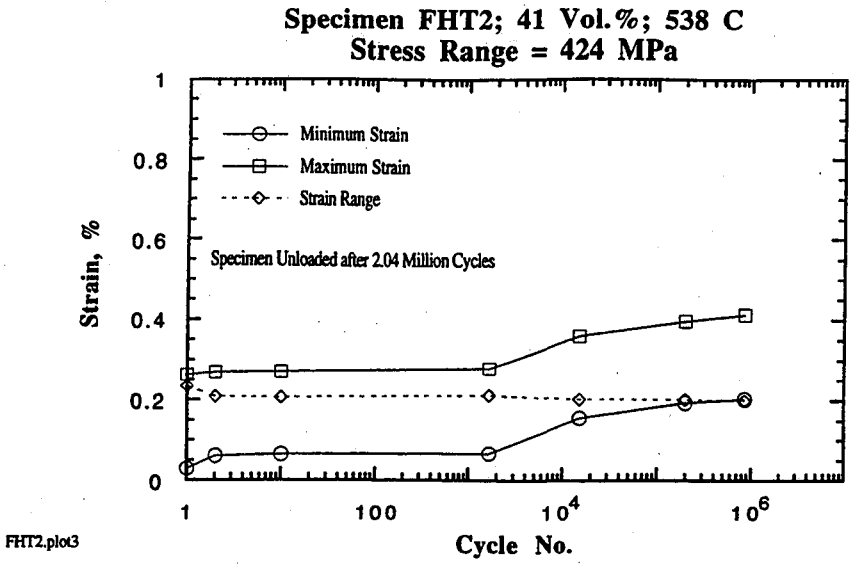

Figure 13b. Evolution of the different strain parameters as a function of the number of cycles for a MMC-41 specimen fatigued at a stress range of 424 MPa at 538 C.

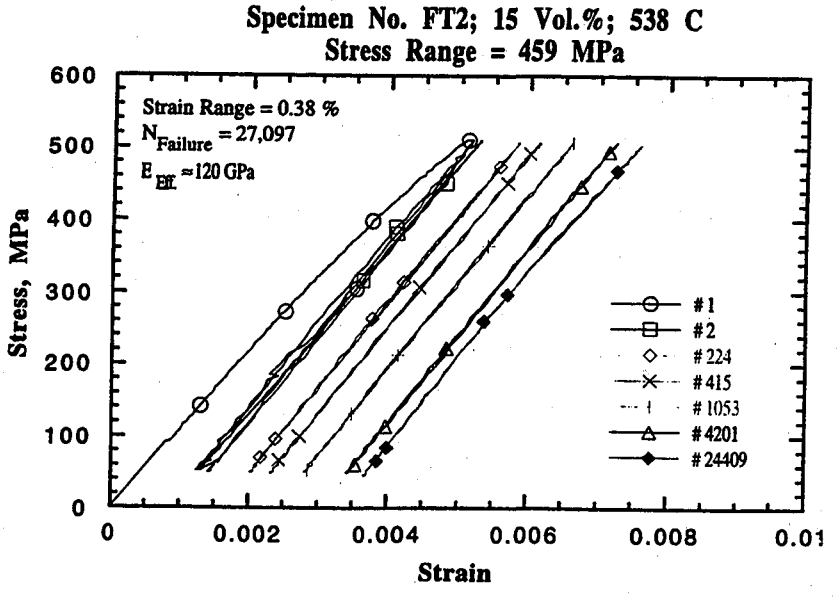

Figure 14a. Stress-strain plots for a MMC-15 specimen cycled at a stress range of 459 MPa at 538 C.

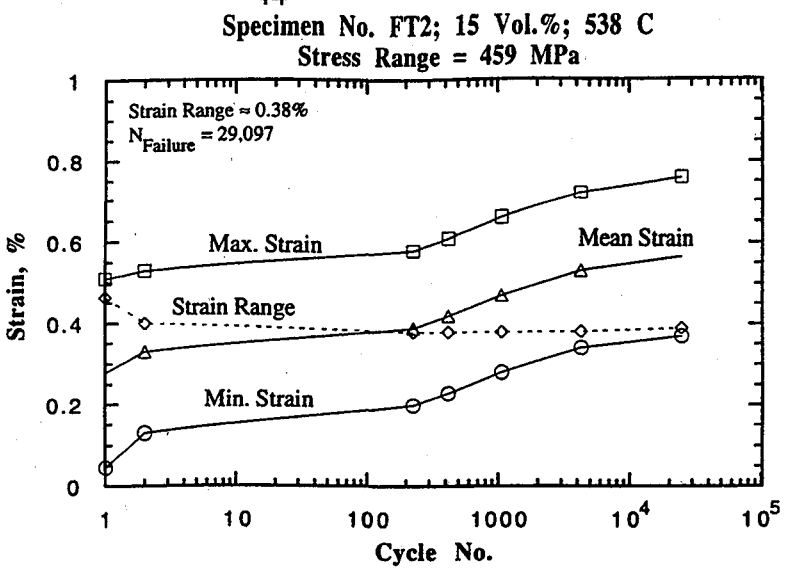

Figure 14b. Evolution of the different strain parameters as a function of the number of cycles for the specimen of Figure 14a.

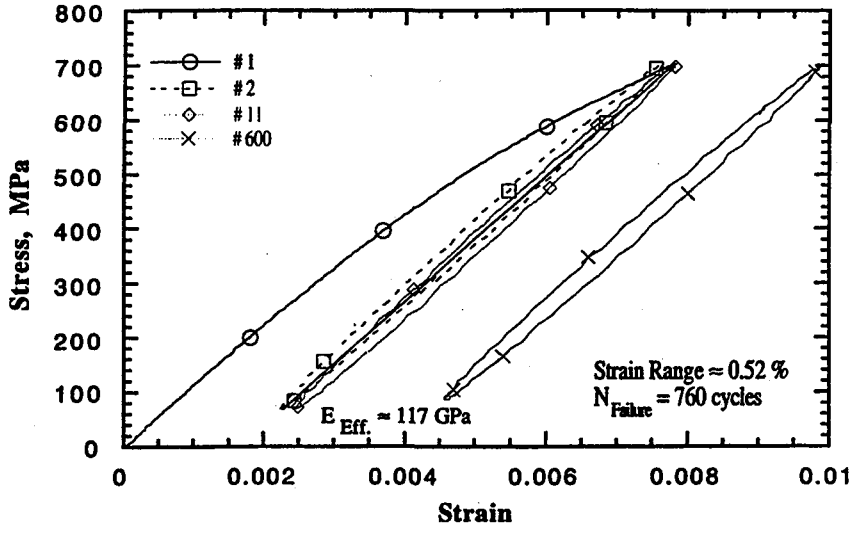

Figure 15a. Stress-strain plots for a MMC-15 specimen cycled at a stress range of 614 MPa at 538 C.

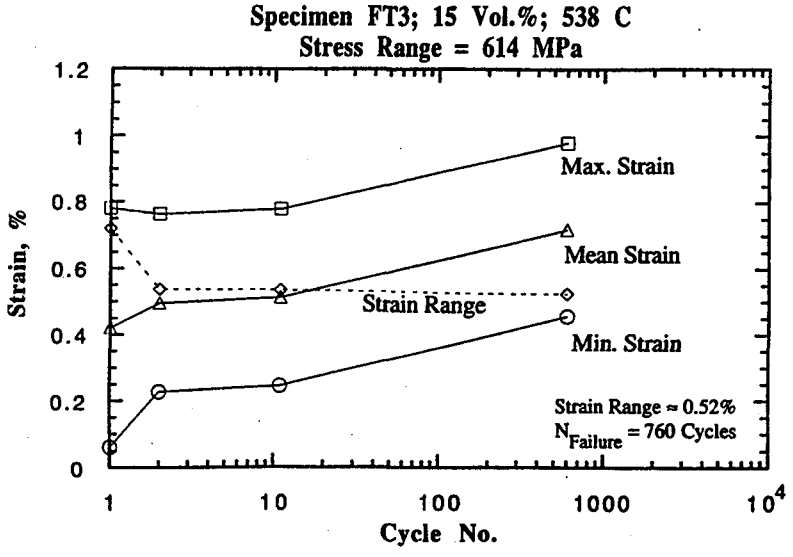

Figure 15b. Evolution of the different strain parameters as a function of the number of cycles for the specimen of Figure 15a.

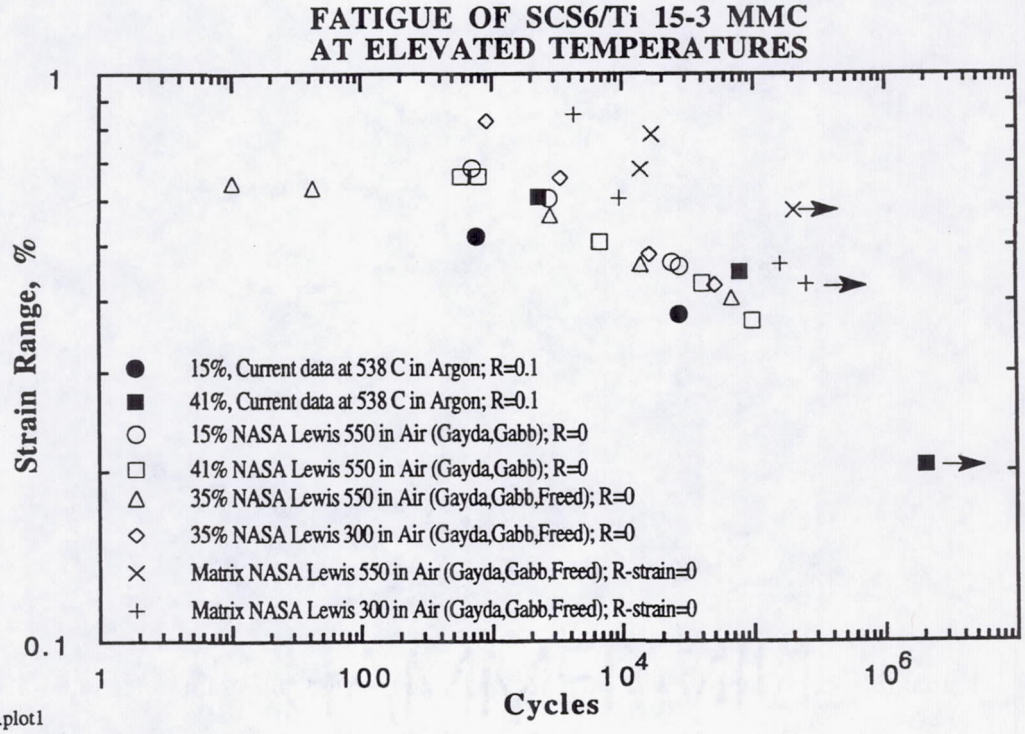

Figure 16. Fatigue life of 0° SCS6/Ti 15-3 specimens tested at elevated temperatures, plotted on a strain range basis. Data for the Ti 15-3 matrix material are also included.

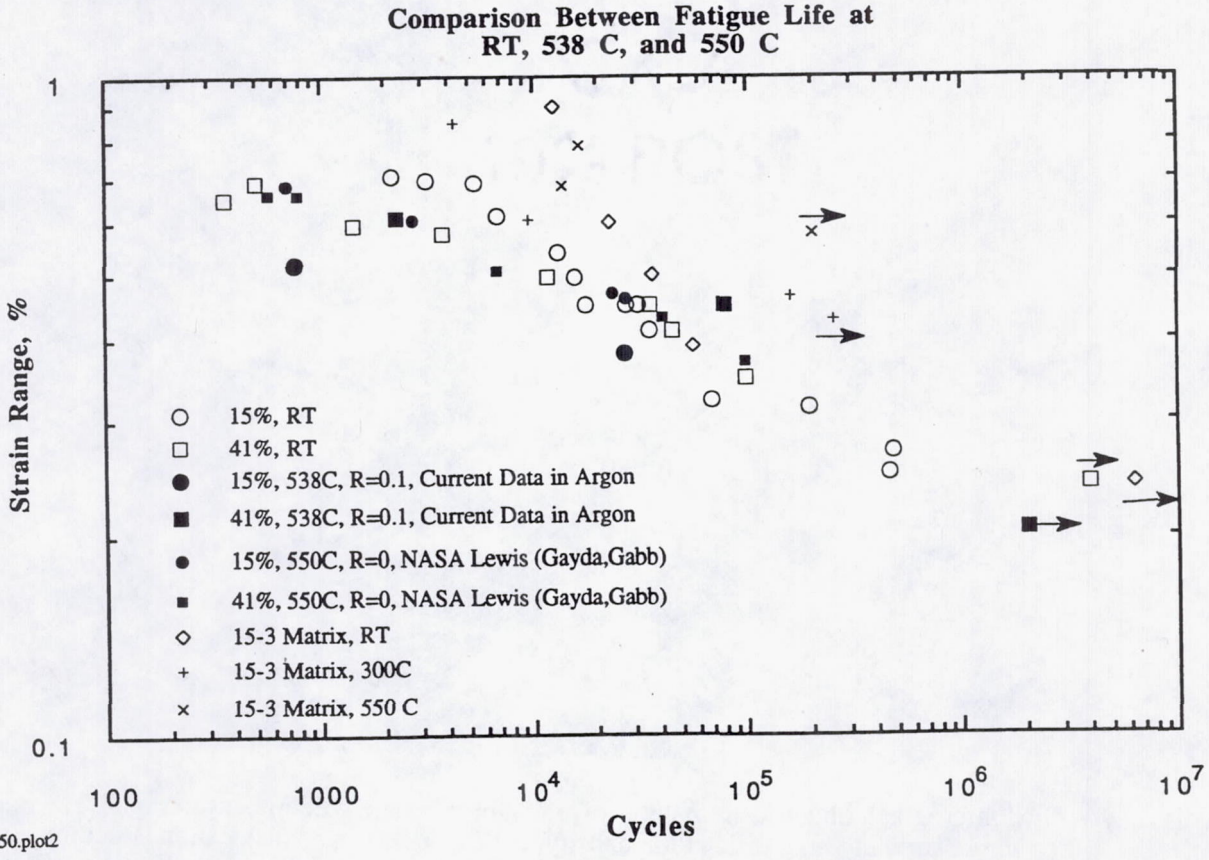

Figure 17. Comparison of fatigue life at RT and elevated temperatrures, on a strain range basis. Data for the Ti 15-3 matrix material also are included.

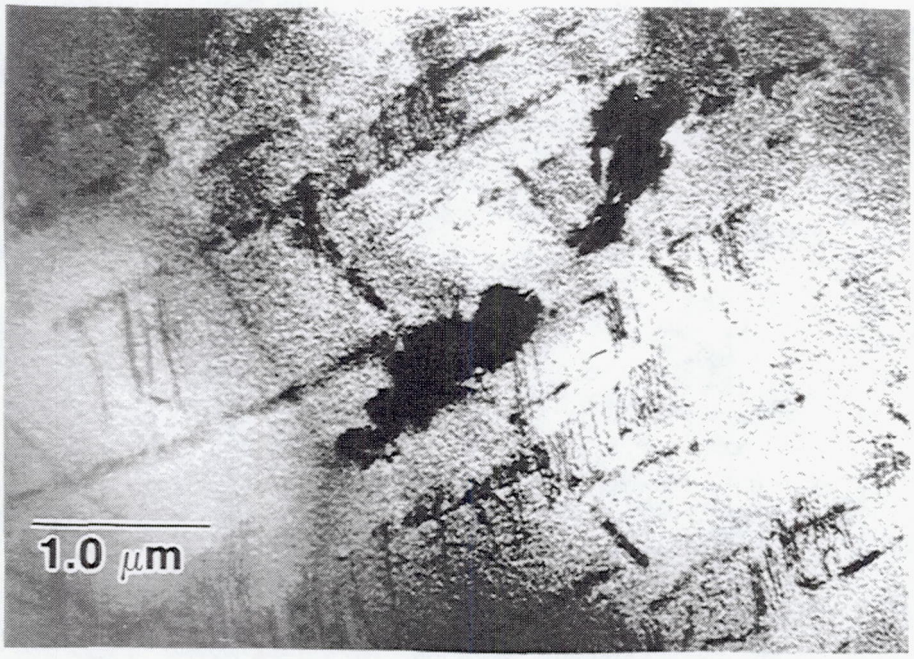

Figure 18. Planar dislocation arrays in a MMC-15 specimen, tested at a strain range of 0.45% at RT.

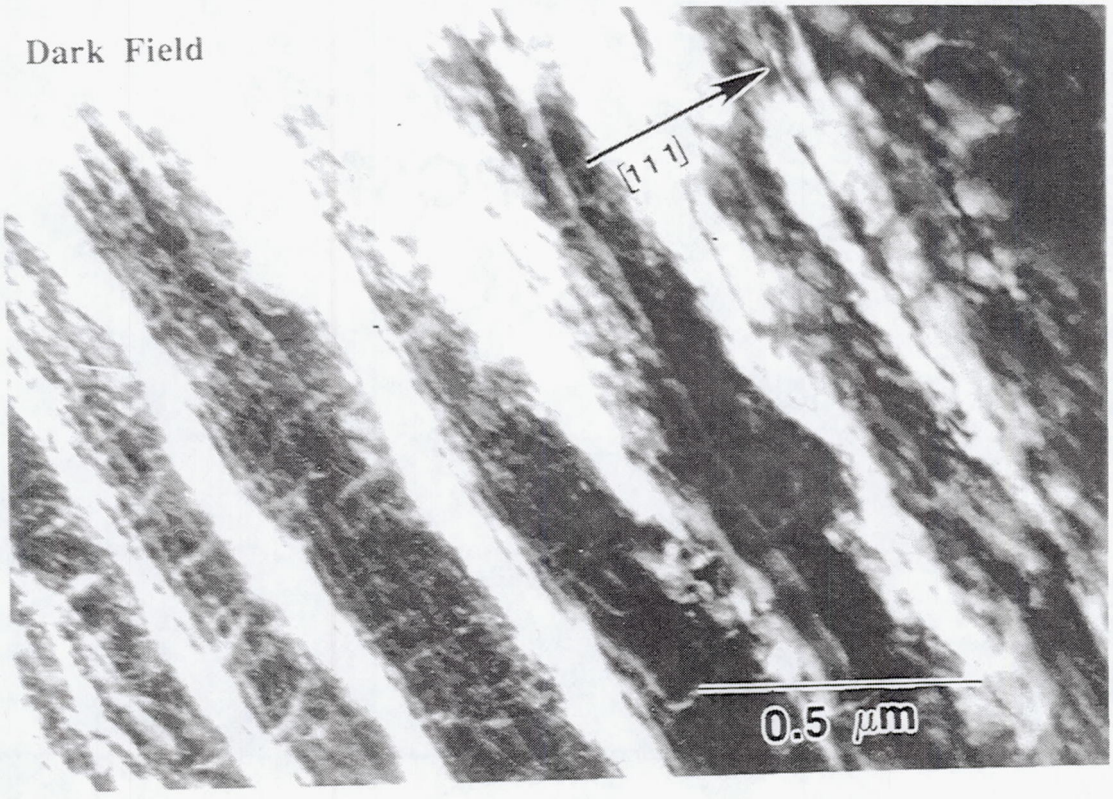

Figure 19. TEM micrograph obtained from another region of the same specimen as in Figure 18, showing extremely high dislocation density, with a channel type dislocation structure. Such dislocation structures are characteristic of persistent slip bands in bcc metals, and confirm that classical fatigue mechanisms operate in the matrix of MMCs.

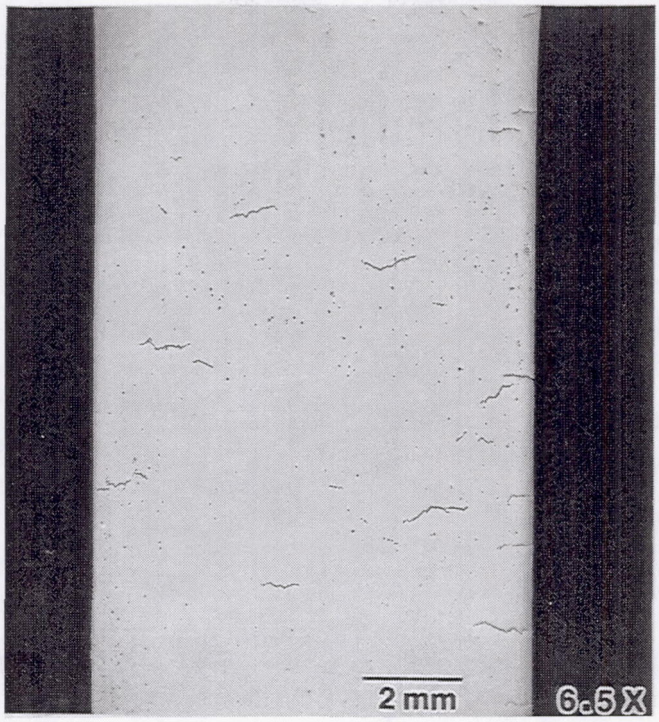

Figure 20a. Photomicrograph illustrating multiple fatigue cracks in a MMC-15 specimen tested at a strain range of 0.45% at RT.

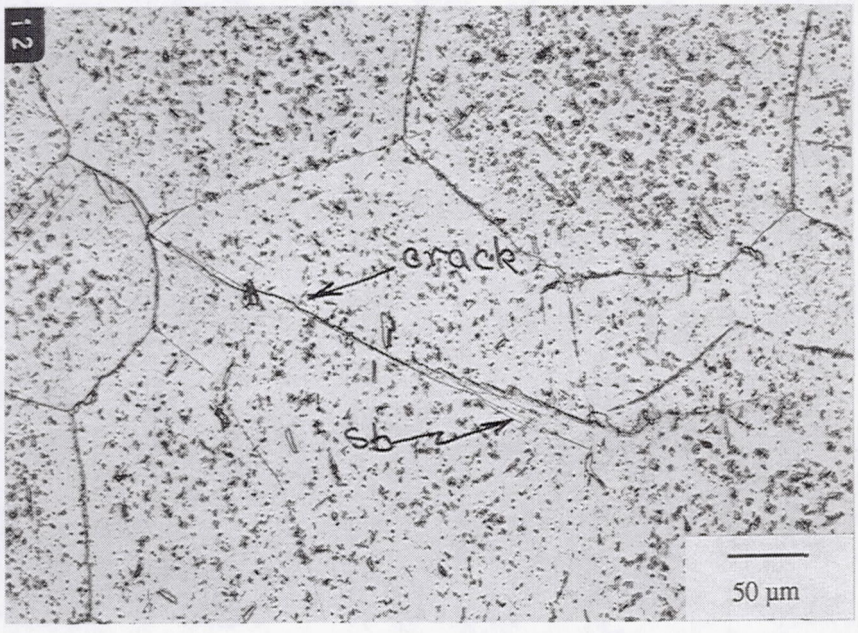

Figure 20b. Crack path and slip bands on the specimen surface, showing the tendency for cracks to follow slip bands at RT; strain range of 0.45% at RT for MMC-15.

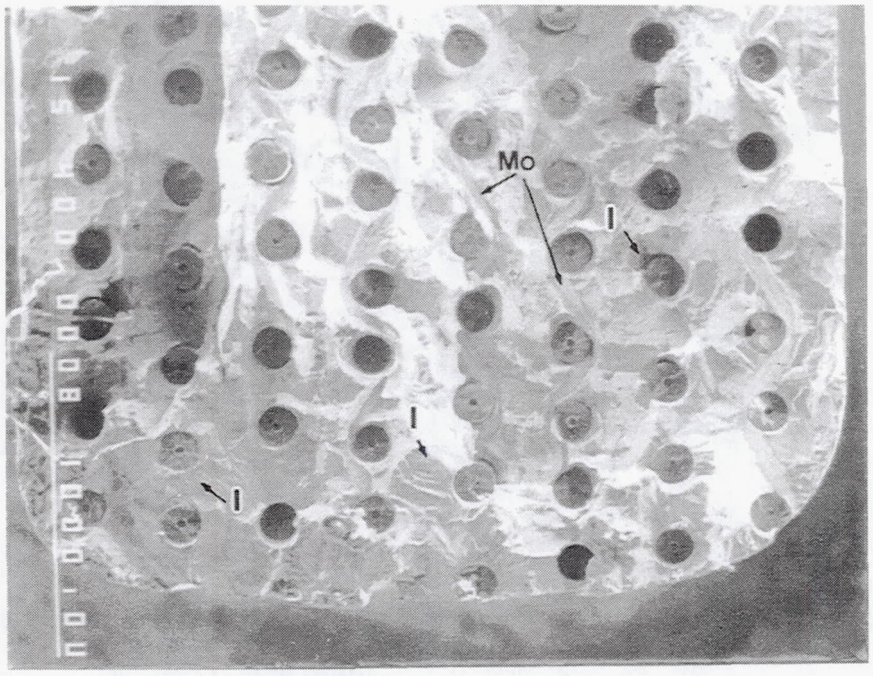

Figure 21. Fractograph of a MMC-15 specimen, cycled at a strain range of 0.45% at RT. The fracture surface revealed large fatigue crack areas, with multiple cracks nucleating from around the fiber; a radial crack initiating from the reaction zone around the fiber is indicated by "I".

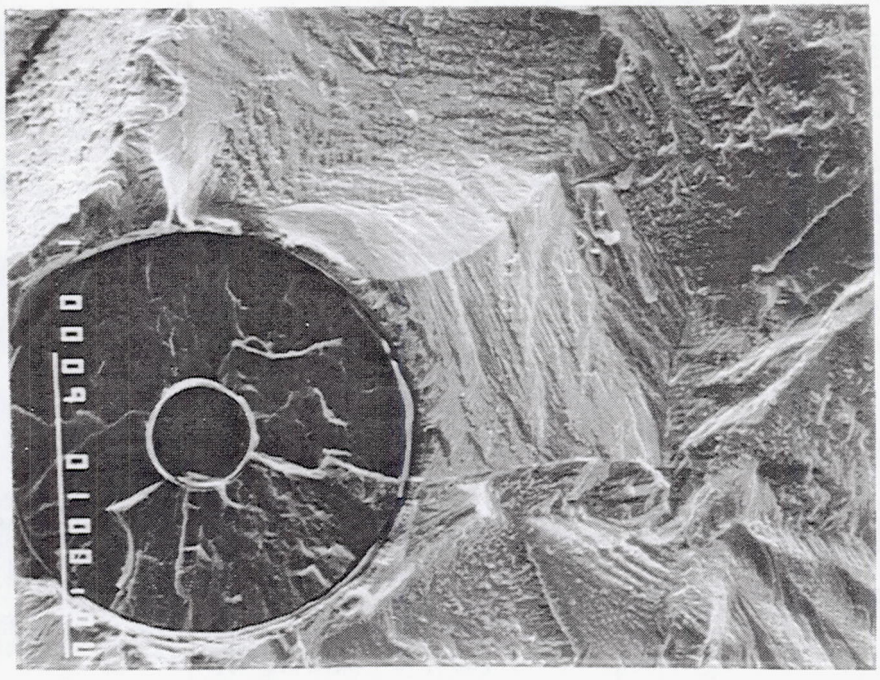

Figure 22. A higher magnification micro graph of the fatigue crack growth region at RT (0.45% strain range), showing the feathery, but crystallographic character of the crack morphology. The side surfaces of the specimen showed that cracks followed slip bands, weaving in and out of parallel and intersecting slip bands.

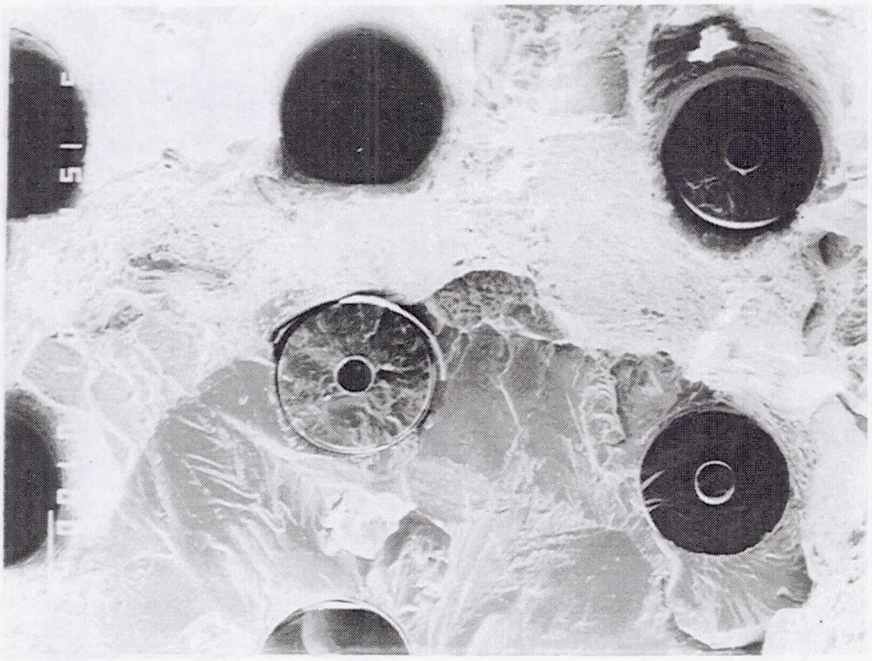

Figure 23. Fractograph taken near the transition regions between fatigue crack growth and fast fracture, in a MMC-15 specimen cycled to failure at RT.

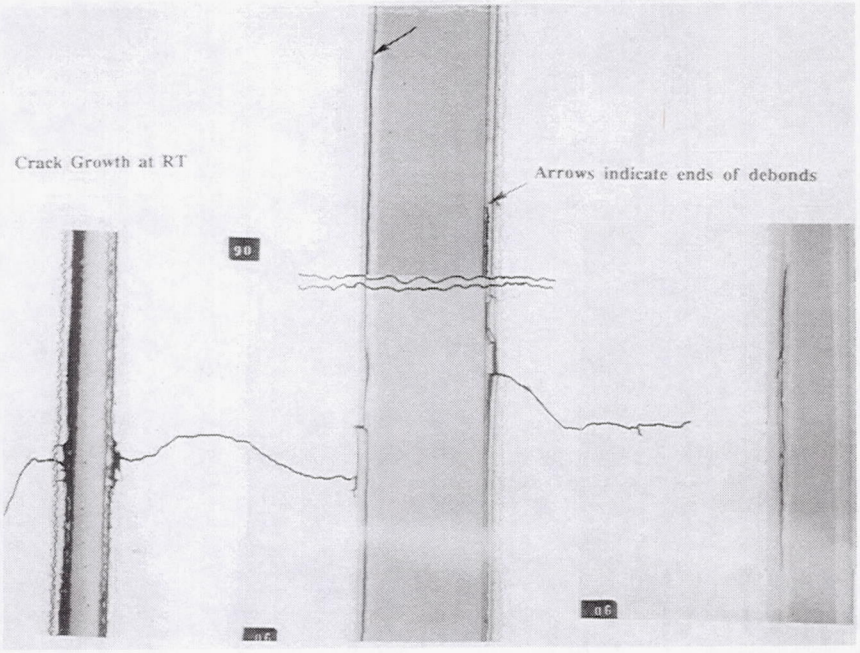

Figure 24. Photograph of a MMC-15 specimen fatigued at a strain range of 0.45% at RT, after the face was polished down to the first set of fibers.

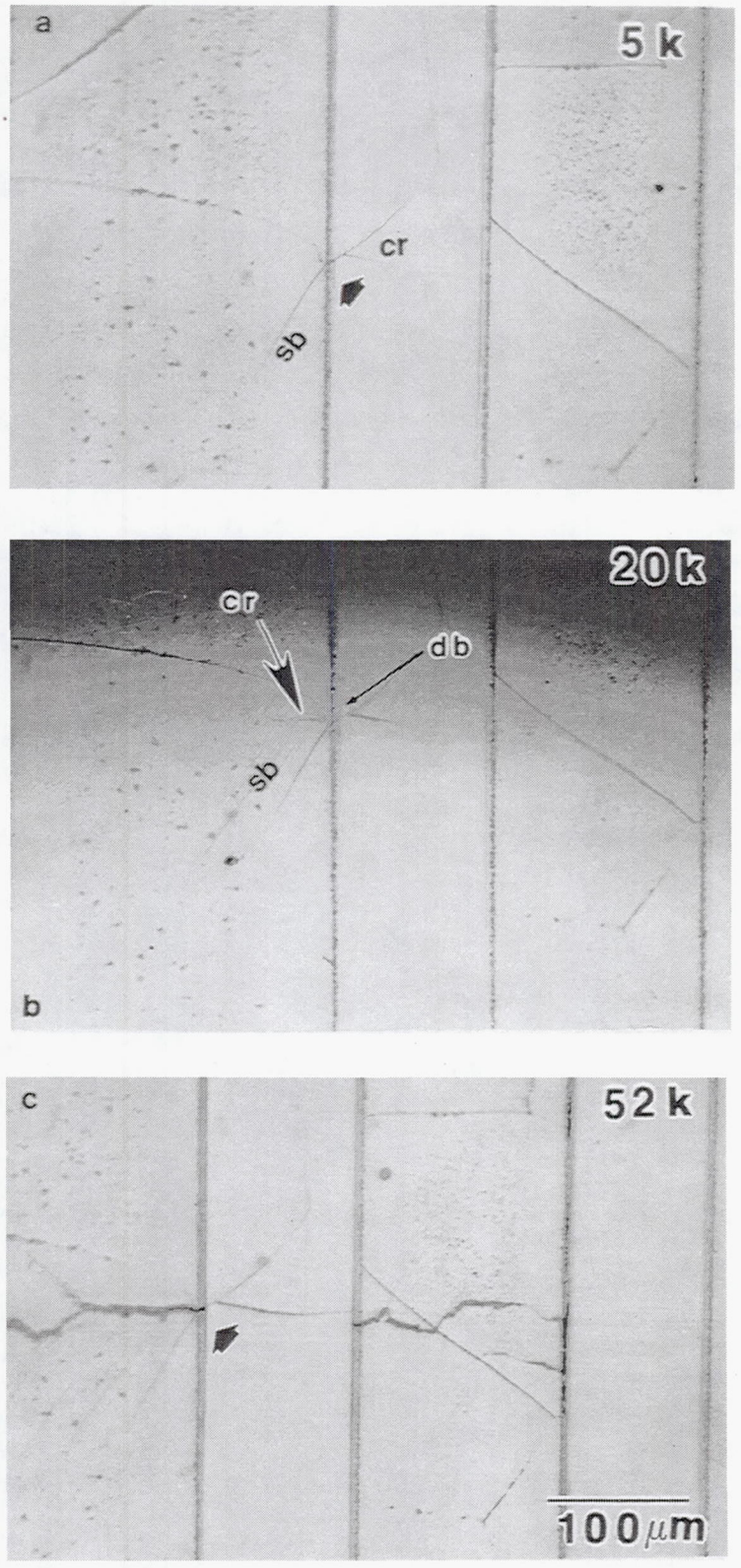

Figure 25. Photographs of replicas of a MMC-15 specimen tested at a strain range of 0.3% at RT. The replicas illustrate the progression of plasticity and damage during fatigue. The cycle numbers are indicated at the top right of each photograph.

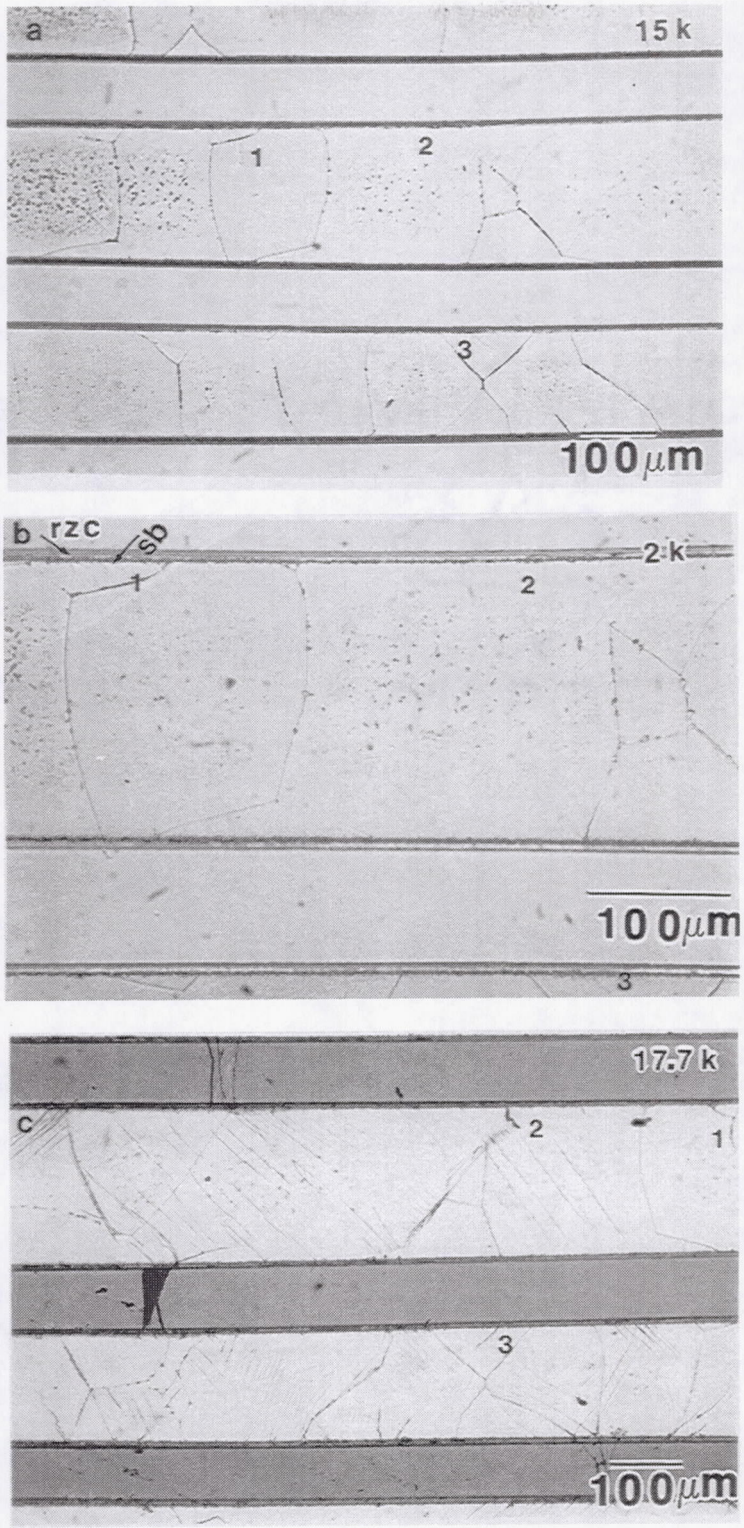

Figure 26. Photographs of replicas and the specimen taken at different fractions of life. The MMC-15 specimen was tested at RT at a strain range of 0.45%, and had been polished down to the first set of fibers before testing. Micrographs (a) and (b) were taken at 15,000 cycles and 2,000 cycles, respectively. Micrograph (c) corresponds to that of the specimen after it had failed.

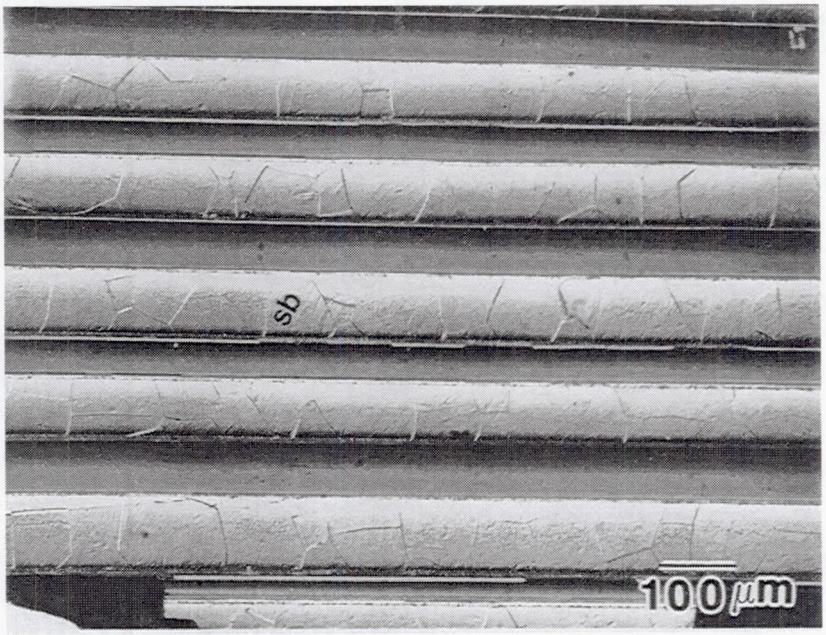

Figure 27. Micrograph of a MMC-41 specimen fatigued at RT at a strain range of 0.62%. The specimen has been polished down to the first set of fibers after its failure in 503 cycles.

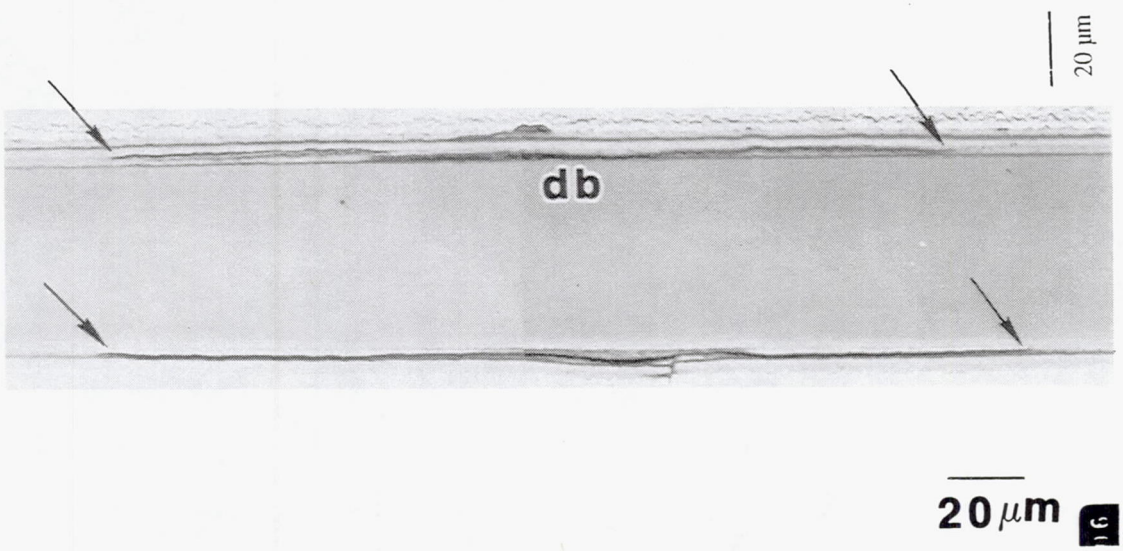

Figure 28a. Debonding around an isolated fiber in a MMC-15 specimen fatigued at a strain range of 0.54% at RT. There were no matrix cracks in the vicinity.

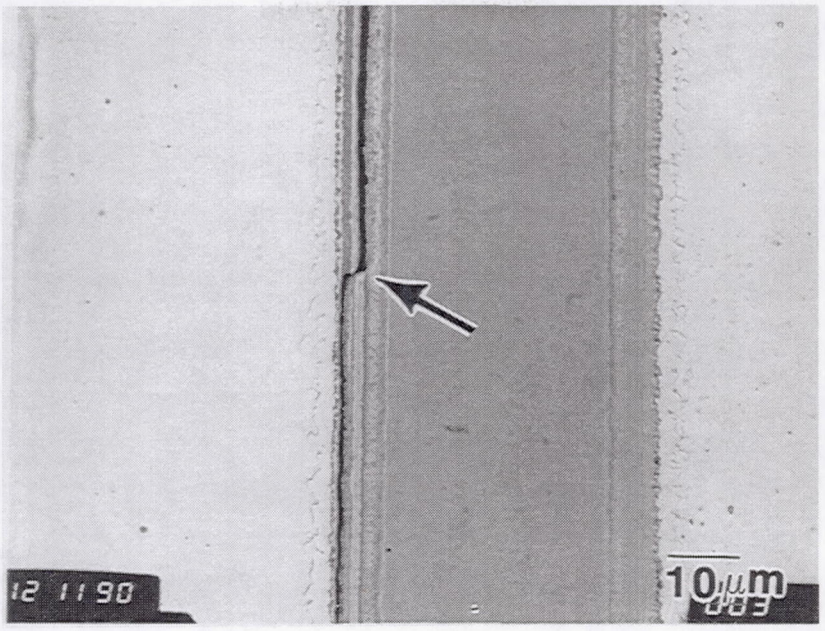

Figure 28b. Close up view of a debond in a MMC-41 specimen cycled at a strain range of 0.69 % at RT. The morphology of the debonding, and the crack in the outer layer of the SCS-6 fiber should be noted.

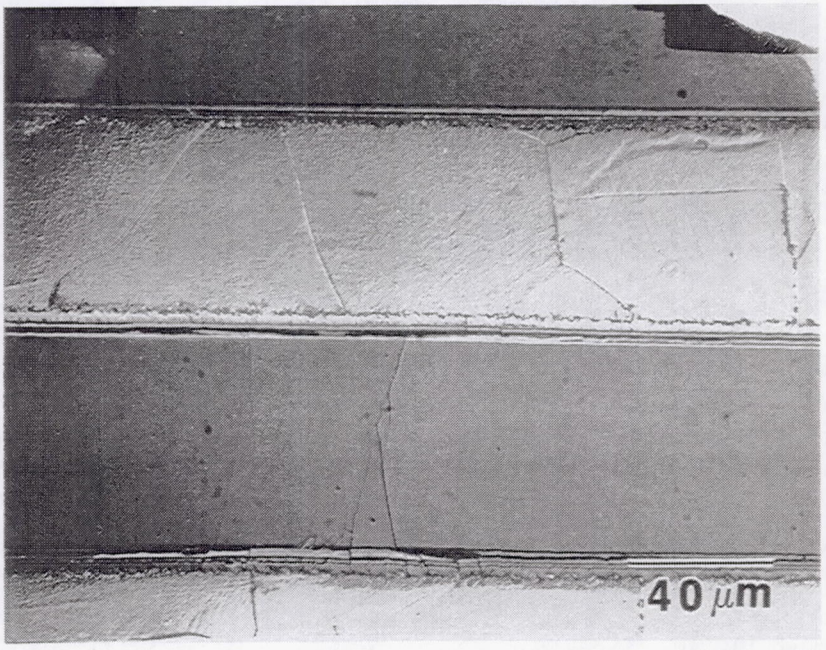

Figure 29a. Fiber crack in a MMC-41 specimen cycled at a strain range of 0.69 % at RT.

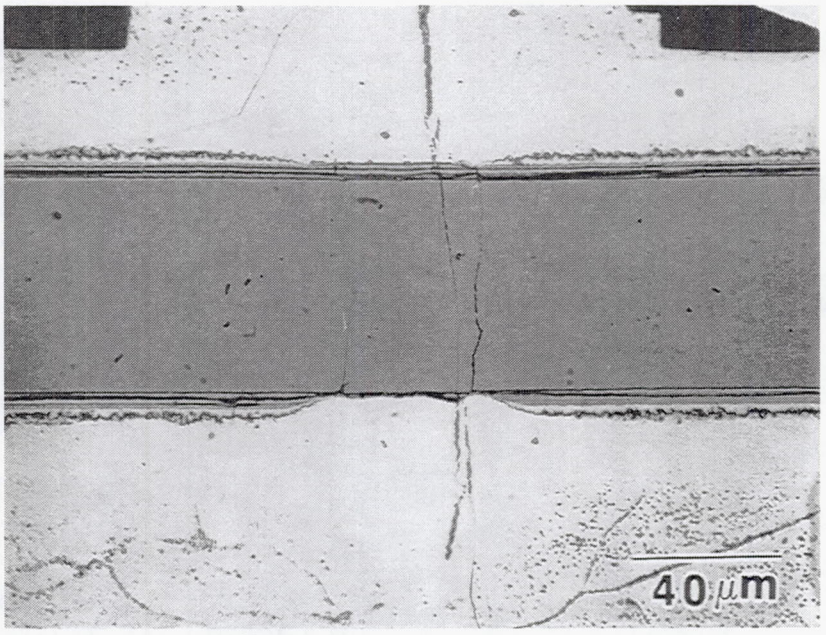

Figure 29b. Close-up view of a fiber crack near a Mo-weave in a MMC-41 specimen fatigued at a strain range of 0.7% at RT. Note how the Mo-weave has reacted with the outer layer of the SCS-6 fiber.

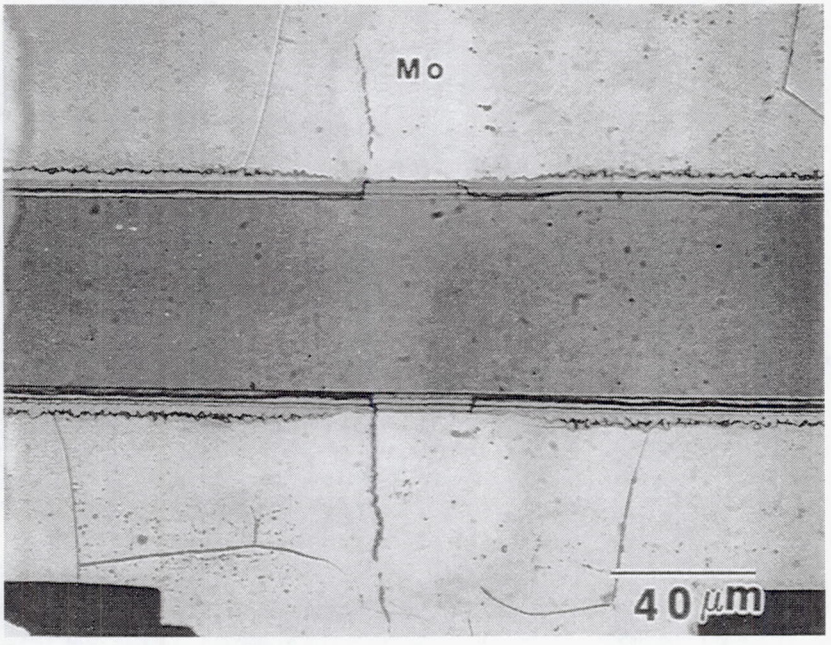

Figure 29c. Cracking of a Mo-weave for the same specimen as in Figure 29a. Note that the fiber has not cracked, and also the outer layers of the SCS-6 fiber are intact.

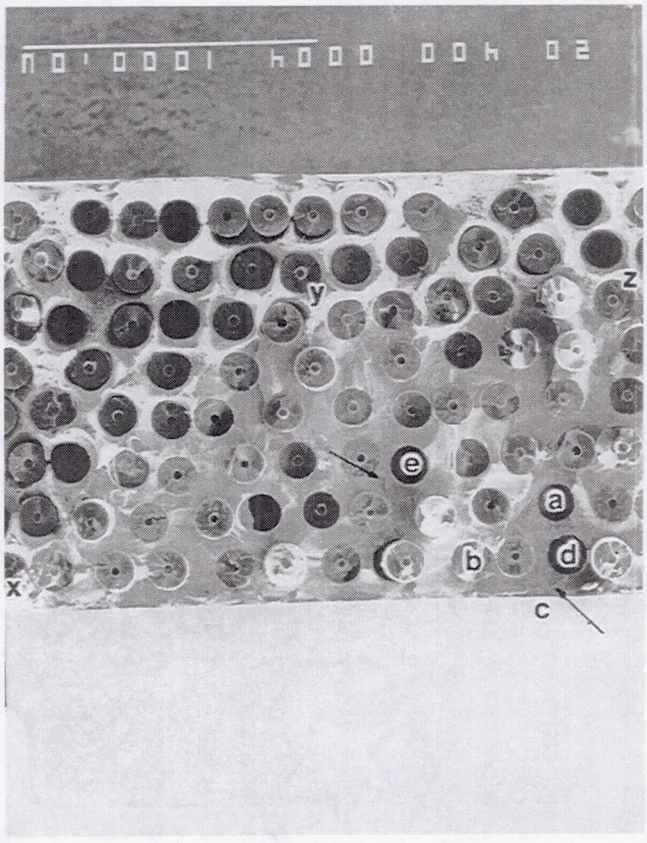

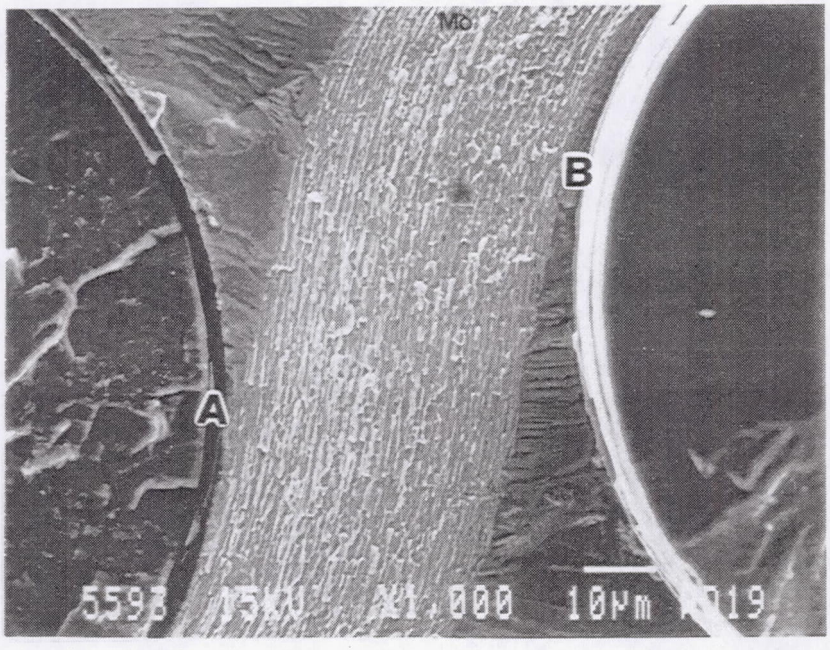

Figure 30. Different views of the fracture surface of a MMC-41 specimen fatigued at a strain range of 0.45% at 538 C. (i) Low magnification view of the fracture surface, and, (ii) high magnification view around a Mo-weave.

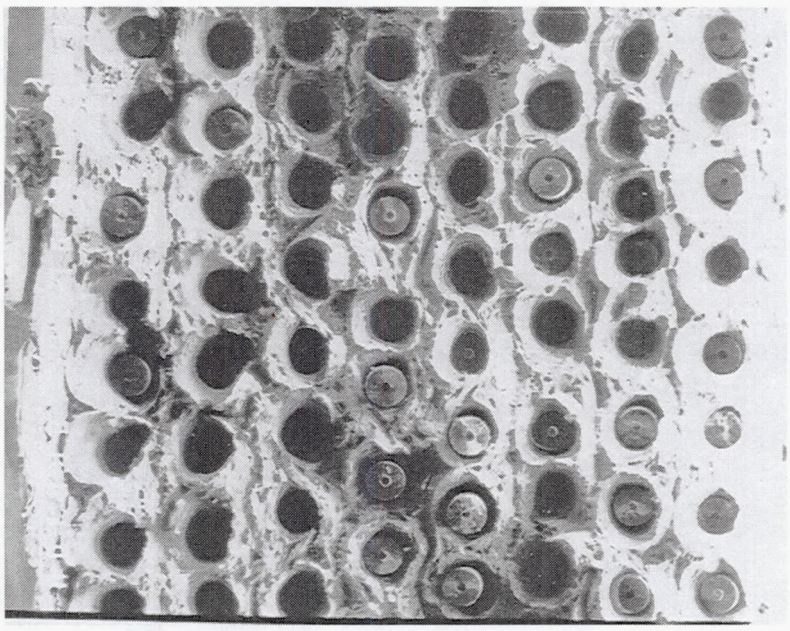

Figure 31. Fracture surface of a MMC-15 specimen that lasted only 760 cycles at a strain range of 0.52% at 538 C.

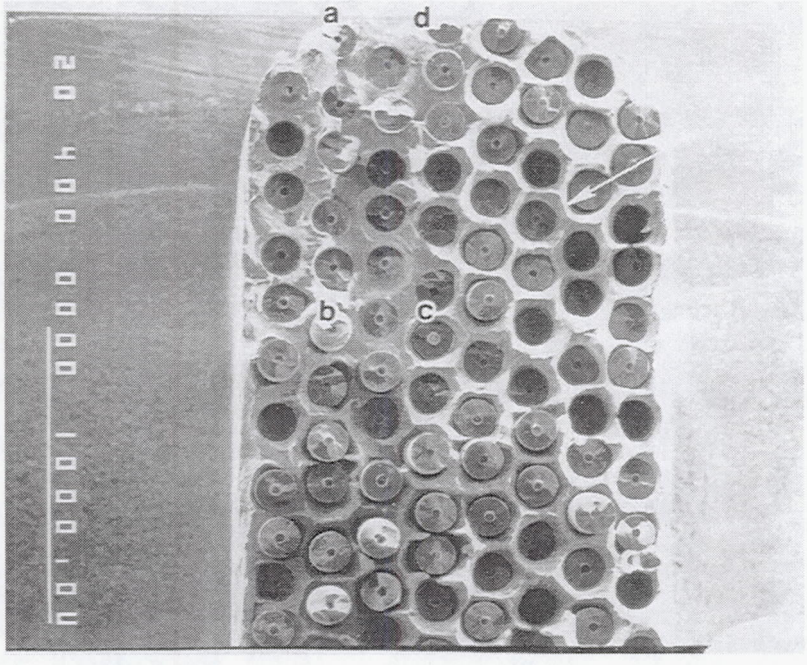

Figure 32. Fracture surface of a MMC-41 specimen tested at a strain range of 0.61% at 538C. The top left (up to the third column from the left surface) shows a fatigue crack region with Mo ribbon visible in many places. The rest of the fracture surface showed ductile-dimple and shear-lip type overload fractures. Note how the matrix has sheared to almost chisel points at mid-regions between fibers in the overload region; the hexagonal symmetry is worth noting.

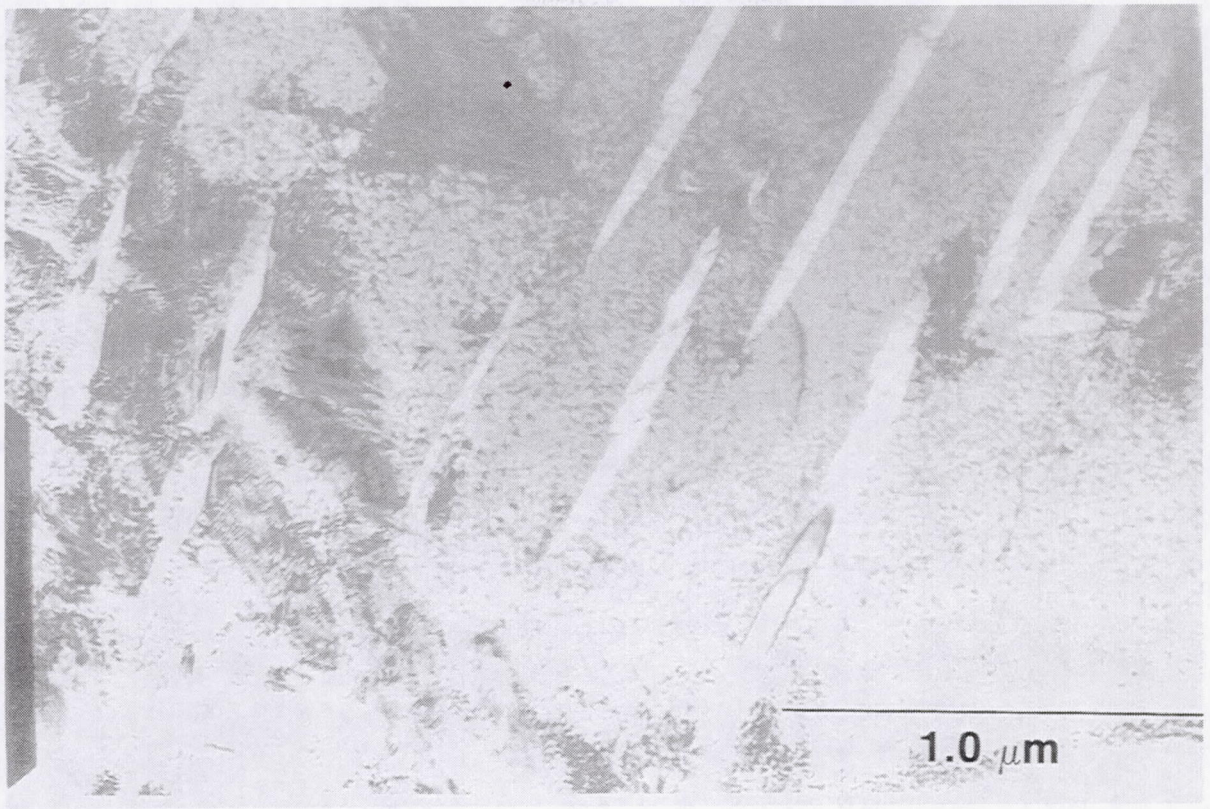

Figure 33. TEM image of the matrix of a MMC-41 specimen fatigued at a strain range of 0.61% at 538 C. The long white particles were identified to be alpha particles, that precipitated insitu during testing. The fringes around certain particles represent interface dislocations.

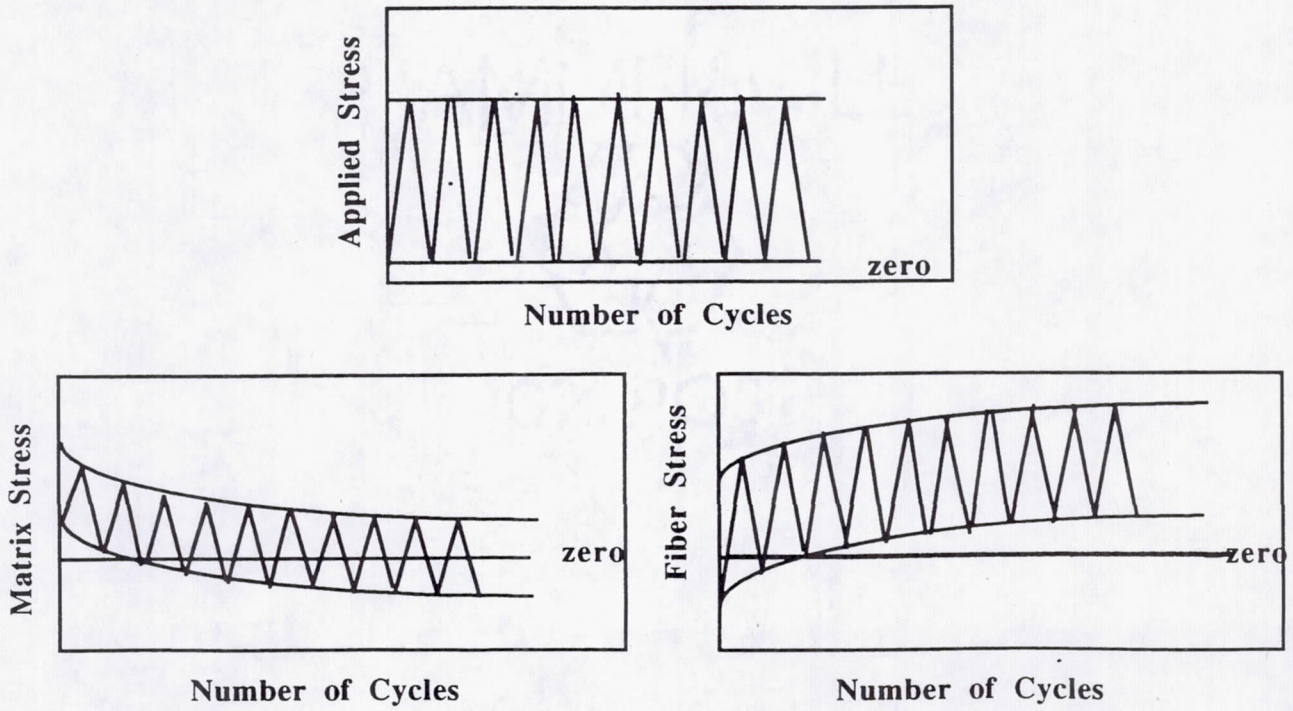

Figure 34. Sketch illustrating how stresses in matrix and fibers change during isothermal fatigue at high temperatures under stress control.

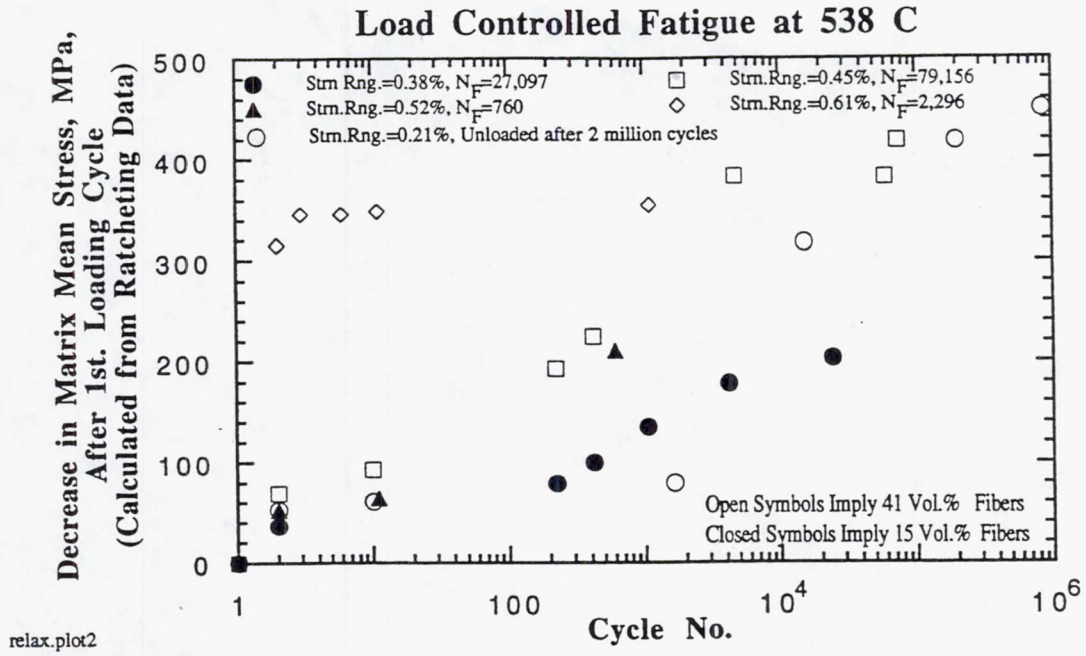

Figure 35. Calculated decrease in the matrix mean stress as a function of the number of cycles in the tests conducted at 538 C. Calculations based on the observed increase in the mean strain.

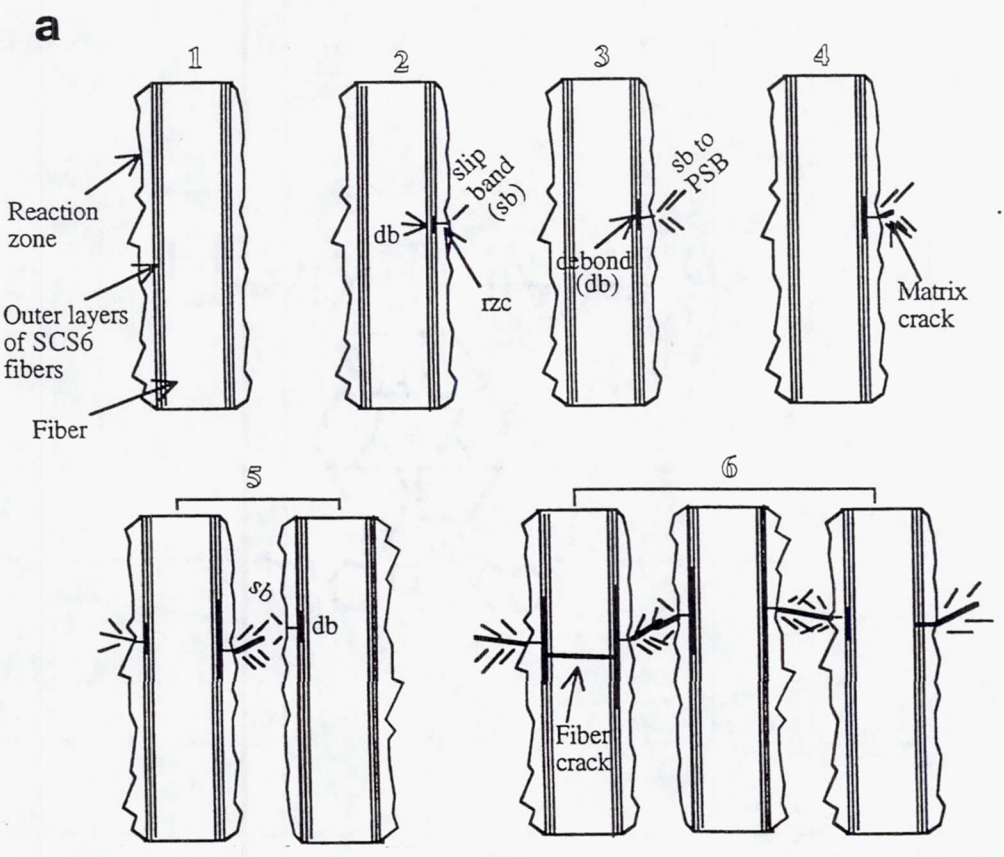

Figure 36. Sketches illustrating our current understanding of the fatigue damage process in Ti-based MMCs. (a) RT, at intermediate strain ranges (Regime 2); (b) RT, at high strain ranges (Regime 1); (c) Elevated temperatures, at intermediate strain ranges (Regime 2); (d) Elevated temperatures, at high strain ranges (Regime 1).

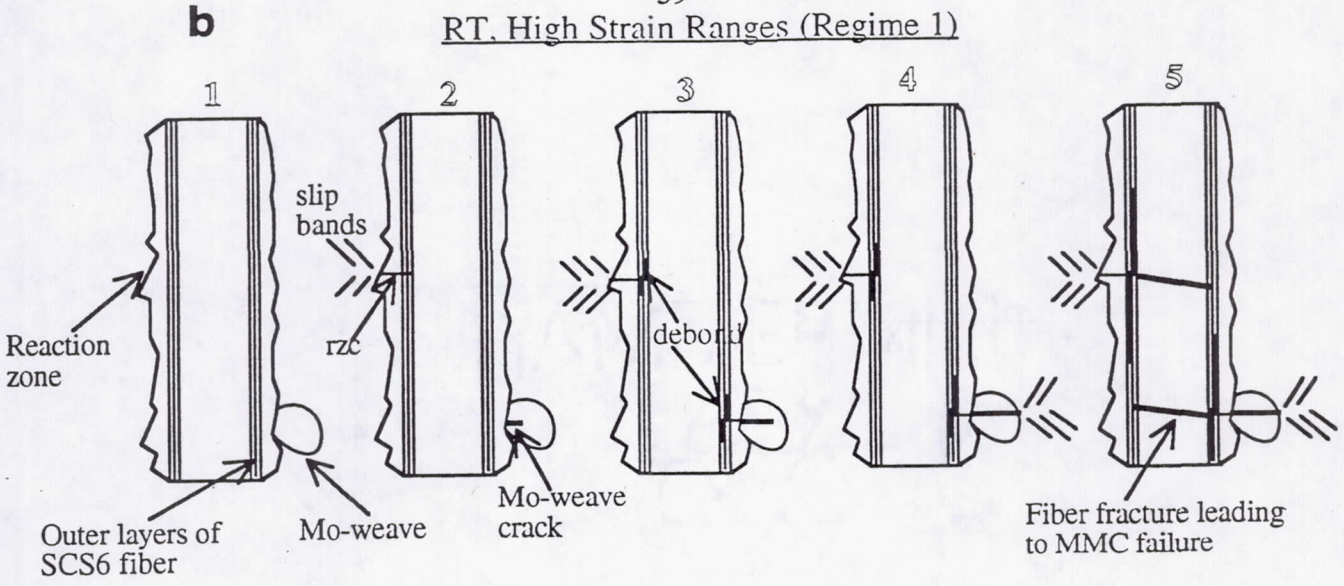

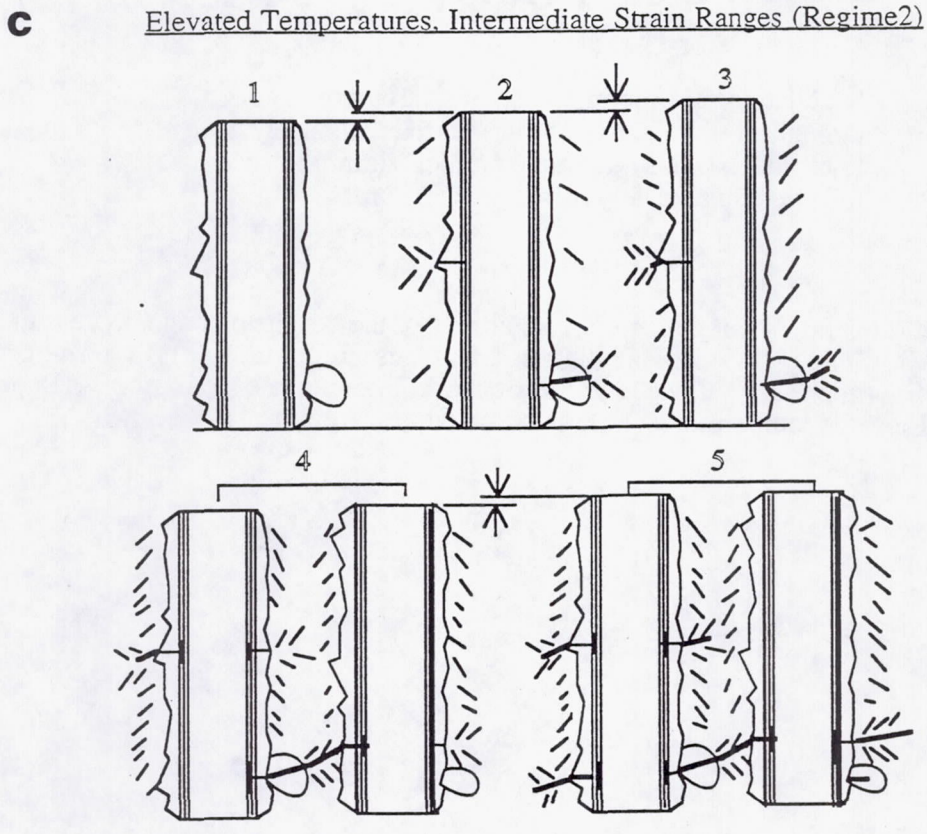

There is a continuous increase in mean strain (ratchetting) with the strain range remaining fairly constant. However, the primary damage mode is matrix cracking, as illustrated here. Both cracked Mo-weaves and reaction-zone cracks are important crack initiating sites, with the former appearing to play a larger role in specimen fracture.

Figure 36. Sketches illustrating our current understanding of the fatigue damage process in Ti-based MMCs. (a) RT, at intermediate strain ranges (Regime 2); (b) RT, at high strain ranges (Regime 1); (c) Elevated temperatures, at intermediate strain ranges (Regime 2); (d) Elevated temperatures, at high strain ranges (Regime 1).

d Elevated Temperatures. At High Strain Ranges (Regime 1)

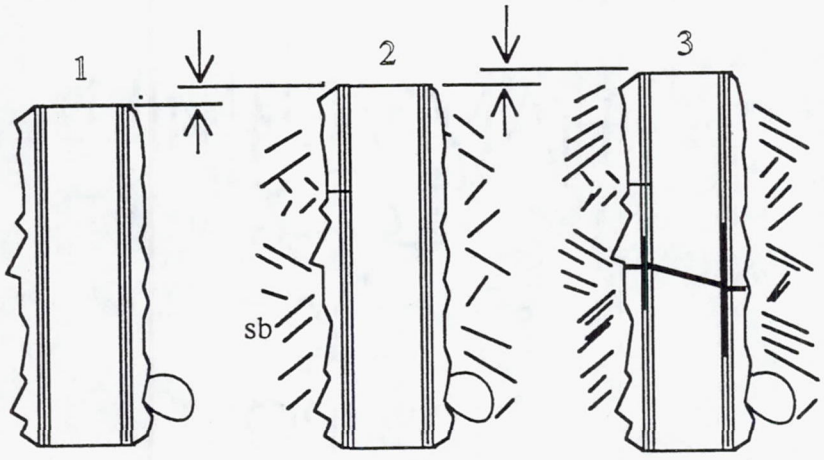

Specimen strains continuously increases from 1 to 3, through stress relaxation of the matrix. Ultimately, the fibers crack (see 3) when their critical strain is reached, followed immediately by specimen failure.

Figure 36. Sketches illustrating our current understanding of the fatigue damage process in Ti-based MMCs. (a) RT, at intermediate strain ranges (Regime 2); (b) RT, at high strain ranges (Regime 1); (c) Elevated temperatures, at intermediate strain ranges (Regime 2); (d) Elevated temperatures, at high strain ranges (Regime 1).

REPORT DOCUMENTATION PAGE

Form Approved
OMB No. 0704-0188

1. AGENCY USE ONLY (*Leave blank*)	2. REPORT DATE	3. REPORT TYPE AND DATES COVERED
	September 1993	Final Contractor Report

4. TITLE AND SUBTITLE

Isothermal Fatigue Mechanisms in Ti-Based Metal Matrix Composites

5. FUNDING NUMBERS

WU–510–01–50
C–NAS3–26494

6. AUTHOR(S)

Bhaskar S. Majumdar and Golam M. Newaz

7. PERFORMING ORGANIZATION NAME(S) AND ADDRESS(ES)

Battelle Memorial Institute
505 King Ave.
Columbus, Ohio 43201–2693

8. PERFORMING ORGANIZATION REPORT NUMBER

E–8086

9. SPONSORING/MONITORING AGENCY NAME(S) AND ADDRESS(ES)

National Aeronautics and Space Administration
Lewis Research Center
Cleveland, Ohio 44135–3191

10. SPONSORING/MONITORING AGENCY REPORT NUMBER

NASA CR–191181

11. SUPPLEMENTARY NOTES

Project Manager, Brad Lerch, Structures Division, (216) 433–5522.

12a. DISTRIBUTION/AVAILABILITY STATEMENT

Unclassified - Unlimited
Subject Category 24

12b. DISTRIBUTION CODE

13. ABSTRACT ***(Maximum 200 words)***

Stress-controlled isothermal fatigue experiments were performed at room temperature (RT) and 548 C (in argon) on $[0]_8$ SCS6/Ti 15-3 metal matrix composites (MMCs) with 15 and 41 volume percent SCS6 (SiC) fibers. The primary objectives were to evaluate the mechanical responses, and to obtain a clear understanding of the damage mechanisms leading to failure of the MMCs. The mechanical data indicated that strain ranges attained fairly constant values in the stress-controlled experiments at both RT and 538 C, and remained so for more than 85% of life. The fatigue data for MMCs with different volume fraction fibers showed that MMC life was controlled by the imposed strain range rather than the stress range. At RT, and at low and intermediate strain ranges, the dominant fatigue mechanism was matrix fatigue, and this was confirmed metallurgically from fractographic evidence as well as from observations of channel type dislocation structures in the matrix of fatigued MMC specimens. Reaction-zone cracks acted as important crack initiating sites at RT, with their role being to facilitate slip band formation and consequent matrix crack initiation through classical fatigue mechanisms. MMC life agreed with matrix life at the lower strain ranges, but was smaller than matrix life at higher strain ranges. Unlike the case of monotonic deformation, debonding damage was another major damage mechanism during fatigue at RT, and it increased for higher strain ranges. At high strain ranges at RT, fractography and metallography showed an absence of matrix cracks, but long lengths of debonds in the outer layers of the SCS6 fibers. Such debonding and consequent rubbing during fatigue is believed to have caused fiber damage and their failure at high strain ranges. Thus, whereas life was matrix dominated at low and intermediate strain ranges, it was fiber dominated at high strain ranges. At 538 C, the mean strain constantly increased (ratchetting) with the number of cycles. At high strain ranges, such ratchetting led to overload failure of the fibers, and debonding of the type at RT was very small. At intermediate strain ranges, fractography showed large areas of matrix cracks. However, in spite of this matrix dominated mechanism, the MMC life at elevated temperatures was significantly less than the matrix fatigue life at all strain ranges. The reason for this difference is still unclear, although metallographic and fractographic evidences suggest that internal crack initiation sites at Mo-ribbons and reaction-zone cracks may have played a critical role, with the former tending to dominate.

14. SUBJECT TERMS

Metal matrix composite; Fatigue; SiC/Ti-15–3; Deformation; Damage

15. NUMBER OF PAGES
62

16. PRICE CODE
A04

17. SECURITY CLASSIFICATION OF REPORT	18. SECURITY CLASSIFICATION OF THIS PAGE	19. SECURITY CLASSIFICATION OF ABSTRACT	20. LIMITATION OF ABSTRACT
Unclassified	Unclassified	Unclassified	